ISSN: 2146-1414

MIRT

Molecular Imaging and Radionuclide Therapy

June 2017 Volume 26 Issue 2 www.tsnm.org

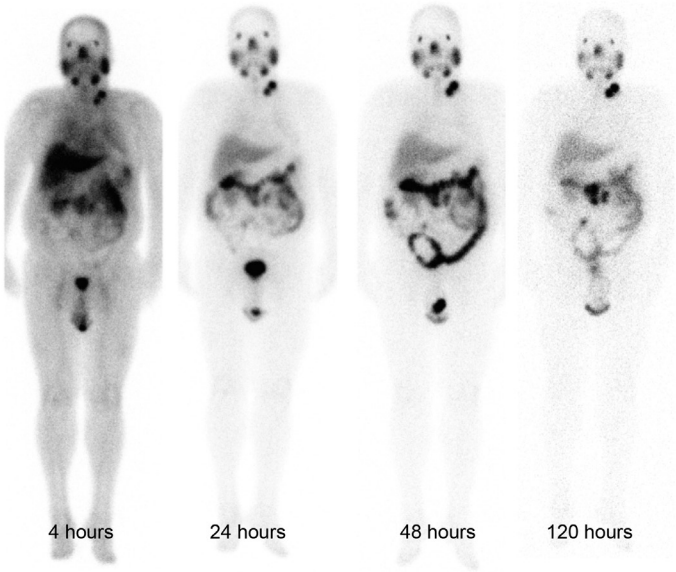

"Official Journal of the Turkish Society of Nuclear Medicine"

galenos yayınevi

TURKISH SOCIETY OF NUCLEAR MEDICINE 1975

MIRT

Molecular Imaging and Radionuclide Therapy

MIRT

Molecular Imaging and Radionuclide Therapy

Cinnah Caddesi Pilot Sokak No: 10/12 Çankaya 06650 Ankara, Turkey +90 312 441 00 45 +90 312 441 12 95 www.tsnm.org dernekmerkezi@tsnm.org
"Formerly Turkish Journal of Nuclear Medicine"

♾ The paper used to print this journal conforms to ISO 9706: 1994 standard (Requirements for Permanence). The National Library of Medicine suggests that biomedical publications be printed on acid-free paper (alkaline paper). Reviewing the articles' conformity to the publishing standards of the Journal, typesetting, reviewing and editing the manuscripts and abstracts in English, creating links to source data, and publishing process are realized by Galenos.

galenos yayınevi

Publisher
Erkan Mor

Publication Director
Nesrin Çolak

Web Coordinators
Eren Arsel
Soner Yıldırım
Turgay Akpınar

Graphics Department
Ayda Alaca
Çiğdem Birinci

Project Coordinators
Ebru Boz
Eda Kolukısa
Hatice Balta
Lütfiye Ayhan İrtem
Melis Kuru
Zeynep Altındağ

Research&Development
Büşrah Toparslan

Finance Coordinator
Sevinç Çakmak

Publisher Contact
Address: Molla Gürani Mah. Kaçamak Sk. No: 21/1 34093 İstanbul, Turkey
Phone: +90 (212) 621 99 25 **Fax:** +90 (212) 621 99 27
E-mail: info@galenos.com.tr/yayin@galenos.com.tr
Web: www.galenos.com.tr

Printing at: Özgün Ofset Ticaret Ltd. Şti.
Yeşilce Mah. Aytekin Sk. No: 21 34418 4. Levent, İstanbul, Turkey
Phone: +90 (212) 280 00 09
Printing Date: June 2017
ISSN: 2146-1414 **E-ISSN:** 2147-1959
International scientific journal published quarterly.

TURKISH SOCIETY OF NUCLEAR MEDICINE 1975

MIRT

Molecular Imaging and Radionuclide Therapy

ABOUT US

Molecular Imaging and Radionuclide Therapy (formerly Turkish Journal of Nuclear Medicine) is the official publication of Turkish Society of Nuclear Medicine.

Focus and Scope

Molecular Imaging and Radionuclide Therapy (Mol Imaging Radionucl Ther, MIRT) is a double-blind peer-review journal published in English language. It publishes original research articles, reviews, editorials, short communications, letters, consensus statements, guidelines and case reports with a literature review on the topic, interesting images in the field of molecular imaging, multimodality imaging, nuclear medicine, radionuclide therapy, radiopharmacy, medical physics, dosimetry and radiobiology. MIRT is published three times a year (February, June, October). Audience: Nuclear medicine physicians, medical physicists, radiopharmaceutical scientists, radiobiologists.

The editorial policies are based on the "Recommendations for the Conduct, Reporting, Editing, and Publication of Scholarly Work in Medical Journals (ICMJE Recommendations)" by the International Committee of Medical Journal Editors (2016, archived at http://www.icmje.org/) rules.

Open Access Policy

This journal provides immediate open access to its content on the principle that making research freely available to the public supports a greater global exchange of knowledge.

Open Access Policy is based on rules of Budapest Open Access Initiative (BOAI) (http://www.budapestopenaccessinitiative.org/). By "open access" to [peer-reviewed research literature], we mean its free availability on the public internet, permitting any users to read, download, copy, distribute, print, search, or link to the full texts of these articles, crawl them for indexing, pass them as data to software, or use them for any other lawful purpose, without financial, legal, or technical barriers other than those inseparable from gaining access to the internet itself. The only constraint on reproduction and distribution, and the only role for copyright in this domain, should be to give authors control over the integrity of their work and the right to be properly acknowledged and cited.

Permission Requests

Instructions for Authors

Instructions for authors are published in the journal and on the website http://mirt.tsnmjournals.org

Manuscripts can only be submitted electronically through the Journal Agent website (http://www.journalagent.com/mirt/?plng=eng) after creating an account. This system allows online submission and review.

All published volumes in full text can be reached free of charge through the website http://mirt.tsnmjournals.org

Material Disclaimer

Scientific and legal responsibilities pertaining to the papers belong to the authors. Contents of the manuscripts and accuracy of references are also the author's responsibility. The Turkish Society of Nuclear Medicine, the Editor, the Editorial Board or the publisher do not accept any responsibility for opinions expressed in articles.

Financial expenses of the journal are covered by Turkish Society of Nuclear Medicine.

Correspondence Address

Editor-in-Chief, Belkis Erbas, MD, Professor in Nuclear Medicine

Hacettepe University, Medical School, Department of Nuclear Medicine,

Ankara, Turkey

Phone: +90 312 441 00 45

Fax: +90 312 441 12 97

E-mail: belkiserbas@tsnmjournals.org

Web page: http://mirt.tsnmjournals.org

Publisher Corresponding Address

Galenos Yayınevi Tic. Ltd. Şti.

Address: Molla Gürani Mah. Kaçamak Sk. No: 21/1 34093

Fındıkzade, İstanbul, Turkey

Phone: +90 212 621 99 25

Fax: +90 212 621 99 27

E-mail: info@galenos.com.tr

The journal is printed on an acid-free paper.

MIRT

Molecular Imaging and Radionuclide Therapy

INSTRUCTIONS TO AUTHORS

Molecular Imaging and Radionuclide Therapy (Mol Imaging Radionucl Ther, MIRT) publishes original research articles, short communications, reviews, editorials, case reports with a literature review on the topic, interesting images, consensus statements, guidelines, letters in the field of molecular imaging, multimodality imaging, nuclear medicine, radionuclide therapy, radiopharmacy, medical physics, dosimetry and radiobiology. MIRT is published by the Turkish Society of Nuclear Medicine three times a year (February, June, October). The journal is printed on an acid-free paper.

Molecular Imaging and Radionuclide Therapy does not charge any article submission or processing fees.

GENERAL INFORMATION

MIRT commits to rigorous peer review, and stipulates freedom from commercial influence, and promotion of the highest ethical and scientific standards in published articles. Neither the Editor(s) nor the publisher guarantees, warrants or endorses any product or service advertised in this publication. All articles are subject to review by the editors and peer reviewers. If the article is accepted for publication, it may be subjected to editorial revisions to aid clarity and understanding without changing the data presented.

Manuscripts must be written in English and must meet the requirements of the journal. The journal is in compliance with the uniform requirements for manuscripts submitted to biomedical journals published by the International Committee of Medical Journal Editors (NEJM 1997; 336:309-315, updated 2016). Manuscripts that do not meet these requirements will be returned to the author for necessary revision before the review. Authors of manuscripts requiring modifications have a maximum of two months to resubmit the revised text. Manuscripts returned after this deadline will be treated as new submissions.

It is the authors' responsibility to prepare a manuscript that meets ethical criteria. The Journal adheres to the principles set forth in the Helsinki Declaration October 2013 (https://www.wma.net/policies-post/wma-declaration-of-helsinki-ethical-principles-for-medical-research-involving-human-subjects/) and holds that all reported research involving "Human beings" conducted in accordance with such principles.

Reports describing data obtained from research conducted in human participants must contain a statement in the MATERIALS AND METHODS section indicating approval by the ethical review board (including the approval number) and affirmation that INFORMED CONSENT was obtained from each participant.

All manuscripts reporting experiments using animals must include a statement in the MATERIALS AND METHODS section giving assurance that all animals have received humane care in compliance with the Guide for the Care and Use of Laboratory Animals (www.nap.edu) and indicating approval by the ethical review board.

If the study should have ethical approval, authors asked to provide ethical approval in order to proceed the review process. If they provide approval, review of the manuscript will continue.

In case report(s) and interesting image(s) a statement regarding the informed consent of the patients should be included in the manuscript and the identity of the patient(s) should be hidden.

Subjects must be identified only by number or letter, not by initials or names. Photographs of patients' faces should be included only if scientifically relevant. Authors must obtain written consent from the patient for use of such photographs.

In cases of image media usage that potentially expose patients' identity requires obtaining permission for publication from the patients or their parents/guardians.

If the proposed publication concerns any commercial product, the author must include in the cover letter a statement indicating that the author(s) has (have) no financial or other interest with the product or explaining the nature of any relations (including consultancies) between the author(s) and editor the manufacturer or distributor of the product.

All submissions will be screened by Crossref Smilarity Check powered by "iThenticate". Manuscripts with an overall similarity index of greater than 25%, or duplication rate at or higher than 5% with a single source will be returned back to authors.

MANUSCRIPT CATEGORIES

1. Original Articles

2. Short Communications are short descriptions of focused studies with important, but very straightforward results.

3. Reviews address important topics in the field. Authors considering the submission of uninvited reviews should contact the editor in advance to determine if the topic that they propose is of current potential interest to the Journal. Reviews will be considered for publication only if they are written by authors who have at least three published manuscripts in the international peer reviewed journals and these studies should be cited in the review. Otherwise only invited reviews will be considered for peer review from qualified experts in the area.

4. Editorials are usually written by invitation of the editor by the editors on current topics or by the reviewers involved in the evaluation of a submitted manuscript and published concurrently with that manuscript.

5. Case Report and Literature Reviews are descriptions of a case or small number of cases revealing a previously undocumented disease process, a unique unreported manifestation or treatment of a known disease process, unique unreported complications of treatment regimens or novel and important insights into a condition's pathogenesis, presentation, and/or management. The journal's policy is to accept case reports only if it is accompanied by a review of the literature on the related topic. They should include an adequate number of images and figures.

6. Interesting Image

One of the regular parts of Molecular Imaging and Radionuclide Therapy is a section devoted to interesting images. Interesting image(s) should describe case(s) which are unique and include interesting findings adding insights into the interpretation of patient images, a condition's pathogenesis, presentation, and/or management.

7. Consensus Statements or Guidelines may be submitted by professional societies. All such submissions will be subjected to peer review, must be modifiable in response to criticisms, and will be published only if they meet the Journal's usual editorial standards.

8. Letters to the Editor may be submitted in response to work that has been published in the Journal. Letters should be short commentaries related to specific points of agreement or disagreement with the published work.

Note on Prior Publication

Articles are accepted for publication on the condition that they are original, are not under consideration by another journal, or have not been previously

MIRT
Molecular Imaging and Radionuclide Therapy

published. Direct quotations, tables, or illustrations that have appeared in copyrighted material must be accompanied by written permission for their use from the copyright owner and authors. Materials previously published in whole or in part shall not be considered for publication. At the time of submission, authors must report that the manuscript has not been published elsewhere. Abstracts or posters displayed at scientific meetings need not be reported.

MANUSCRIPT SUBMISSION PROCEDURES

MIRT only accepts electronic manuscript submission at the web site http://www.journalagent.com/mirt/. After logging on to the website Click the 'online manuscript submission' icon. All corresponding authors should be provided with a password and a username after entering the information required. If you already have an account from a previous submission, enter your username and password to submit a new or revised manuscript. If you have forgotten your username and/or password, please send an e-mail to the editorial office for assistance. After logging on to the article submission system please read carefully the directions of the system to give all needed information and attach the manuscript, tables and figures and additional documents.

All Submissions Must Include:

1. Completed Copyright Assignment & Disclosure of Potential Conflict of Interest Form; This form should be downloaded from the website (provided in the author section), filled in thoroughly and uploaded to the website during the submission.
2. All manuscripts describing data obtained from research conducted in human participants must be accompanied with an approval document by the ethical review board.
3. All manuscripts reporting experiments using animals must include approval document by the animal ethical review board.
4. All submissions must include the authorship contribution form which is signed by all authors.

Authors must complete all online submission forms. If you are unable to successfully upload the files please contact the editorial office by e-mail.

MANUSCRIPT PREPARATION

General Format

The Journal requires that all submissions be submitted according to these guidelines:

- Text should be double spaced with 2.5 cm margins on both sides using 12-point type in Times Roman font.
- All tables and figures must be placed after the text and must be labeled.
- Each section (abstract, text, references, tables, figures) should start on a separate page.
- Manuscripts should be prepared as a word document (*.doc) or rich text format (*.rtf).
- Please make the tables using the table function in Word.
- Abbreviations should be defined in parenthesis where the word is first mentioned and used consistently thereafter.
- Results should be expressed in metric units. Statistical analysis should be done accurately and with precision. Please consult a statistician if necessary.
- Authors' names and institutions should not be included in the manuscript text and should be written only in the title page.

Title Page

The title page should be a separate form from the main text and should include the following:

- Full title (in English and in Turkish). Turkish title will be provided by the editorial office for the authors who are not Turkish speakers.
- Authors' names and institutions.
- Short title of not more than 40 characters for page headings.
- At least three and maximum eight keywords. (in English and in Turkish). Do not use abbreviations in the keywords. Turkish keywords will be provided by the editorial office for the authors who are not Turkish speakers. If you are not a native Turkish speaker, please reenter your English keywords to the area provided for the Turkish keywords. English keywords should be provided from http://www.nlm.nih.gov/mesh (Medical Subject Headings) while Turkish keywords should be provided from http://www.bilimterimleri.com.
- Word count (excluding abstract, figure legends and references).
- Corresponding author's e-mail and address, telephone and fax numbers.
- Name and address of person to whom reprint requests should be addressed.

Original Articles

Authors are required to state in their manuscripts that ethical approval from an appropriate committee and informed consents of the patients were obtained.

Original Articles should be submitted with a structured abstract of no more than 250 words. All information reported in the abstract must appear in the manuscript. The abstract should not include references. Please use complete sentences for all sections of the abstract. Structured abstract should include background, objective, methods, results and conclusions. Turkish abstract will be provided by the editorial office for the authors who are not Turkish speakers. If you are not a native Turkish speaker, please reenter your English abstract to the area provided for the Turkish abstract.

- Introduction
- Materials and Methods
- Results
- Discussion
- Study Limitations
- Conclusion

May be given for contributors who are not listed as authors, or for grant support of the research.

References should be cited in numerical order (in parentheses) in the text and listed in the same numerical order at the end of the manuscript on a separate page or pages. The author is responsible for the accuracy of references. Examples of the reference style are given below. Further examples will be found in the articles describing the Uniform Requirements for Manuscripts Submitted to Biomedical Journals (Ann Intern Med.1988; 208:258-265, Br Med J. 1988; 296:401-405). The titles of journals should be abbreviated according to the style used in the Index Medicus. Journal Articles and Abstracts: Surnames and initials of author's name, title of the article, journal name, date, volume number, and pages. All authors should be listed regardless of number. The citation of unpublished papers, observations or personal communications is not permitted. Citing an abstract is

not recommended. Books: Surnames and initials of author's names, chapter title, editor's name, book title, edition, city, publisher, date and pages.

Sample References

Journal Article: Sayit E, Söylev M, Capa G, Durak I, Ada E, Yilmaz M. The role of technetium-99m-HMPAO-labeled WBC scintigraphy in the diagnosis of orbital cellulitis. Ann Nucl Med 2001;15:41-44.

Erselcan T, Hasbek Z, Tandogan I, Gumus C, Akkurt I. Modification of Diet in Renal Disease equation in the risk stratification of contrast induced acute kidney injury in hospital inpatients. Nefrologia 2009 doi: 10.3265/Nefrologia.2009.29.5.5449.en.full.

Article in a journal published ahead of print: Ludbrook J. Musculovenous pumps in the human lower limb. Am Heart J 2009;00:1-6. (accessed 20 February 2009).

Lang TF, Duryea J. Peripheral Bone Mineral Assessment of the Axial Skeleton: Technical Aspects. In: Orwoll ES, Bliziotes M (eds). Osteoporosis: Pathophsiology and Clinical Management. New Jersey, Humana Pres Inc, 2003;83-104.

Books: Greenspan A. Orthopaedic Radiology a Pratical Approach. 3th ed. Philadelphia, Lippincott Williams Wilkins 2000, 295-330.

Website: Smith JR. 'Choosing Your Reference Style', Online Referencing 2(3), http://orj.sagepub.com (2003, accessed October 2008).

- Tables

Tables must be constructed as simply as possible. Each table must have a concise heading and should be submitted on a separate page. Tables must not simply duplicate the text or figures. Number all tables in the order of their citation in the text. Include a title for each table (a brief phrase, preferably no longer than 10 to 15 words). Include all tables in a single file following the manuscript.

– Figure Legends

Figure legends should be submitted on a separate page and should be clear and informative.

– Figures

Number all figures (graphs, charts, photographs, and illustrations) in the order of their citation in the text. At submission, the following file formats are acceptable: AI, EMF, EPS, JPG, PDF, PPT, PSD, TIF. Figures may be embedded at the end of the manuscript text file or loaded as separate files for submission. All images MUST be at or above intended display size, with the following image resolutions: Line Art 800 dpi, Combination (Line Art + Halftone) 600 dpi, Halftone 300 dpi. Image files also must be cropped as close to the actual image as possible.

Short Communications:

Short communications should be submitted with a structured abstract of no more than 200 words. These manuscripts should be no longer than 2000 words, and include no more than two figures and tables and 20 references. Other rules which the authors are required to prepare and submit their manuscripts are the same as described above for the original articles.

Review Articles:

- Title page (see above)
- Abstract: Maximum 250 words; without structural divisions; in English and in Turkish . Turkish abstract will be provided by the editorial office for the authors who are not Turkish speakers. If you are not a native Turkish speaker, please reenter your English abstract to the area provided for the Turkish abstract.
- Text
- Conclusion
- Acknowledgements (if any)
- References

Editorial:

- Title page (see above)
- Abstract: Maximum 250 words; without structural divisions; in English and in Turkish. Turkish abstract will be provided by the editorial office for the authors who are not Turkish speakers. If you are not a native Turkish speaker, please re enter your English abstract to the area provided for the Turkish abstract.
- Text
- References

Case Report and Literature Review

- Title page (see above)
- Abstract: Approximately 100-150 words; without structural divisions; in English and in Turkish. Turkish abstract will be provided by the editorial office for the authors who are not Turkish speakers. If you are not a native Turkish speaker, please re-enter your English abstract to the area provided for the Turkish abstract.
- Introduction
- Case report
- Literature Review and Discussion
- References

Interesting Image:

No manuscript text is required. Interesting Image submissions must include the following:

Title Page: (see Original article section)

Abstract: Approximately 100-150 words; without structural divisions; in English and in Turkish. Turkish abstract will be provided by the editorial office for the authors who are not Turkish speakers. If you are not a native Turkish speaker, please re-enter your English abstract to the area provided for the Turkish abstract.

Image(s): The number of images is left to the discretion of the author. (See Original article section)

Figure Legend: Reference citations should appear in the legends, not in the abstract. Since there is no manuscript text, the legends for illustrations should be prepared in considerable detail but should be no more than 500 words total. The case should be presented and discussed in the Figure legend section.

References: Maximum eight references (see original article section).

Letters to the Editor:

- Title page (see above)
- Short comment to a published work, no longer than 500 words, no figures or tables.
- References no more than five.

Consensus Statements or Guidelines: These manuscripts should typically be no longer than 4000 words and include no more than six figures and tables and 120 references.

MIRT
Molecular Imaging and Radionuclide Therapy

INSTRUCTIONS TO AUTHORS

Proofs and Reprints

Proofs and a reprint orders are sent to the corresponding author. The author should designate by footnote on the title page of the manuscript the name and address of the person to whom reprint requests should be directed. The manuscript when published will become the property of the journal.

Archiving

The editorial office will retain all manuscripts and related documentation (correspondence, reviews, etc.) for 12 months following the date of publication or rejection.

Submission Preparation Checklist

As part of the submission process, authors are required to check off their submission's compliance with all of the following items, and submissions may be returned to authors that do not adhere to these guidelines.

1. The submission has not been previously published, nor is it before another journal for consideration (or an explanation has been provided in Comments to the Editor).
2. The submission file is in Microsoft Word, RTF, or WordPerfect document file format. The text is double-spaced; uses a 12-point font; employs italics, rather than underlining (except with URL addresses); and the location for all illustrations, figures, and tables should be marked within the text at the appropriate points.
3. Where available, URLs for the references will be provided.
4. All authors should be listed in the references, regardless of the number.
5. The text adheres to the stylistic and bibliographic requirements outlined in the Author Guidelines, which is found in About the Journal.
6. English keywords should be provided from http://www.nlm.nih.gov/mesh(Medical Subject Headings), while Turkish keywords should be provided fromhttp://www.bilimterimleri.com
7. The title page should be a separate document from the main text and should be uploaded separately.
8. The "Affirmation of Originality and Assignment of Copyright/The Disclosure Form for Potential Conflicts of Interest Form" and Authorship Contribution Form should be downloaded from the website, filled thoroughly and uploaded during the submission of the manuscript.

TO AUTHORS

Copyright Notice

The author(s) hereby affirms that the manuscript submitted is original, that all statement asserted as facts are based on author(s) careful investigation and research for accuracy, that the manuscript does not, in whole or part, infringe any copyright, that it has not been published in total or in part and is not being submitted or considered for publication in total or in part elsewhere. Completed Copyright Assignment & Affirmation of Originality Form will be uploaded during submission. By signing this form;

1. Each author acknowledges that he/she participated in the work in a substantive way and is prepared to take public responsibility for the work.
2. Each author further affirms that he or she has read and understands the "Ethical Guidelines for Publication of Research".
3. The author(s), in consideration of the acceptance of the manuscript for publication, does hereby assign and transfer to the Molecular Imaging and Radionuclide Therapy all of the rights and interest in and the copyright of the work in its current form and in any form subsequently revised for publication and/or electronic dissemination.

Privacy Statement

The names and email addresses entered in this journal site will be used exclusively for the stated purposes of this journal and will not be made available for any other purpose or to any other party.

Peer Review Process

1. The manuscript is assigned to an editor, who reviews the manuscript and makes an initial decision based on manuscript quality and editorial priorities.
2. For those manuscripts sent for external peer review, the editor assigns at least two reviewers to the manuscript.
3. The reviewers review the manuscript.
4. The editor makes a final decision based on editorial priorities, manuscript quality, and reviewer recommendations.
5. The decision letter is sent to the author.

Contact Address

All correspondence should be directed to the Editorial Office:
Cinnah Caddesi Pilot Sokak No:10/12 06650 Çankaya / Ankara, Turkey
Phone: +90 312 441 00 45
Fax: +90 312 441 12 97
E-mail: info@tsnmjournals.org

MIRT
Molecular Imaging and Radionuclide Therapy

CONTENTS

Original Articles

47 ^{18}F-FDG-PET/CT in Initiation and Progression of Inflammation and Infection
Enfeksiyon ve Enflamasyonun Oluşum ve Gelişim Sürecinin ^{18}F-FDG-PET/BT Kullanılarak İzlenmesi
Türkan Ertay, Mine Sencan Eren, Meral Karaman, Gülgün Oktay, Hatice Durak; İzmir, Turkey

53 Experimental and Simulation Analysis of Radiation of the Beta Emitting Sources in a Magnetic Field
Manyetik Alanda Beta Yayan Kaynakların Işınımının Deneysel ve Simülasyon Analizi
Berrin Çavuşoğlu, Selda Sucu, Hatice Durak, Kadir Akgüngör, Hakan Epik, Türkan Ertay; İzmir, Turkey

62 Lu-177-PSMA-617 Prostate-Specific Membrane Antigen Inhibitor Therapy in Patients with Castration-Resistant Prostate Cancer: Stability, Bio-distribution and Dosimetry
Kastrasyona Dirençli Prostat Kanseri Hastalarında Lu-177-PSMA-617 ile Prostat Spesifik Membran Antijen İnhibitor Tedavisi: Kararlılık, Biyodağılım ve Dozimetri
Levent Kabasakal, Türkay Toklu, Nami Yeyin, Emre Demirci, Mohammad Abuqbeitah, Meltem Ocak, Aslan Aygün, Emre Karayel, Hüseyin Pehlivanoğlu, Nalan Alan Selçuk; İstanbul, Turkey

69 Efficacy of ^{18}F-2-fluoro-2-deoxy-D-glucose Positron Emission Tomography/Computerized Tomography for Bone Marrow Infiltration Assessment in the Initial Staging of Lymphoma
^{18}F-2-fluoro-2-deoksi-D-glukoz Pozitron Emisyon Tomografisi/Bilgisayarlı Tomografinin Lenfomanın İnisiyal Evrelemesinde Kemik İliği Tutulumunun Belirlenmesindeki Rolü
Ali Ozan Öner, Evrim Sürer Budak, Funda Aydın, Ozan Salim, Orhan Kemal Yücel, Bahar Akkaya, Tayfur Toptaş, Adil Boz, Akın Yıldız, Fırat Güngör, Levent Undar; Afyonkarahisar, Antalya, İstanbul, Turkey

76 Clinical Significance of ^{18}F-Fluorodeoxyglucose Avid Prostate Gland Incidentalomas on Positron Emission Tomography/Computed Tomography
Pozitron Emisyon Tomografisi/Bilgisayarlı Tomografide ^{18}F-Fluorodeoksiglukoz Avid Prostat Bezi İnsidentalomalarının Klinik Önemi
William Makis, Anthony Ciarallo; Edmonton, Montreal, Canada

Original Article
Mol Imaging Radionucl Ther 2017;26:47-52 DOI:10.4274/mirt.18291

^{18}F-FDG-PET/CT in Initiation and Progression of Inflammation and Infection

Enfeksiyon ve Enflamasyonun Oluşum ve Gelişim Sürecinin ^{18}F-FDG-PET/BT Kullanılarak İzlenmesi

Türkan Ertay[1], Mine Sencan Eren[1], Meral Karaman[2], Gülgün Oktay[3], Hatice Durak[1]
[1]Dokuz Eylül University Faculty of Medicine, Department of Nuclear Medicine, İzmir, Turkey
[2]Dokuz Eylül University Faculty of Medicine, Department of Clinical Microbiology, İzmir, Turkey
[3]Dokuz Eylül University Faculty of Medicine, Department of Clinical Biochemistry, İzmir, Turkey

Abstract

Objective: Detection/localization of infection and inflammation is important for the initiation of correct treatment as well as its maintenance. Nuclear medicine imaging methods play an important role in determining infection and inflammation. ^{18}F-2'-deoxy-2-fluoro-d-glucose (^{18}F-FDG) positron emission tomography/computed tomography (PET/CT) is highly sensitive in such cases when used with tomographic cross-sections. In this study, the development and progression of infection and inflammation were monitored on rats by using ^{18}F-FDG via PET/CT.

Methods: Sterile and infected abscesses were formed on rats using turpentine and *S. aureus*, respectively. For evaluation of the formation and progression of the abscess, ^{18}F-FDG was injected into the rats and they were imaged by PET/CT at intervals of twenty-four hours for five days. Maximum standard uptake value (SUV_{max}) of ^{18}F-FDG was calculated.

Results: The highest activity involvement was seen on the first day of abscess formation. On the first day, SUV_{max} of the *S. aureus* abscess was 3.9±0.9 while in the sterile abscess SUV_{max} in the first day was 2.2±0.8. ^{18}F-FDG uptake decreased day by day and it reached the background level on the fourth and fifth days. There were statistically significant differences between *S. aureus* and sterile abscess, and between sterile abscess and background activity in terms of SUV_{max} values during the first three days ($p<0.05$). On the fourth and fifth days, there was no statistically significant difference between *S. aureus* and sterile abscess, and between sterile abscess and background activity ($p>0.05$).

Conclusion: The results demonstrated that the SUV_{max} value for ^{18}F-FDG can be useful in the early differentiation of sterile and infected abscess. In addition, ^{18}F-FDG-PET imaging has the advantage of local availability of equipment and labeled agents leading rapid diagnosis of differentiation of infection and inflammation.

Keywords: Abscess, infection, inflammation, *S. aureus*, turpentine, positron emission tomography/computed tomography, ^{18}F-2'-deoxy-2-fluoro-d-glucose, rat

Öz

Amaç: Enfeksiyon ve enflamasyonun tespit edilmesi ve yerinin belirlenmesi, doğru tedavinin başlanması ve hastaların bakımı için birincil öneme sahiptir. Enfeksiyon ve enflamasyonu saptamada nükleer tıp görüntüleme yöntemleri önemli rol oynar. ^{18}F-2'-deoksi-2-fluoro-d-glukoz (^{18}F-FDG) pozitron emisyon tomografisi/bilgisayarlı tomografi (PET/BT) yüksek duyarlılığa sahiptir. Bu çalışmada enfeksiyon ve enflamasyonun oluşum ve gelişim süreci ^{18}F-FDG ile PET/BT kullanılarak izlendi.

Address for Correspondence: Türkan Ertay MD, Dokuz Eylül University Faculty of Medicine, Department of Nuclear Medicine, İzmir, Turkey
Phone: +90 232 412 42 80 E-mail: turkan.ertay@gmail.com **Received:** 20.01.2015 **Accepted:** 13.03.2017

Öz

Yöntem: Terebentin ve *S. aureus* kullanılarak ratlarda steril ve enfekte apse oluşturuldu. Apsenin oluşum ve gelişim sürecini değerlendirmek için ratlar 24 saatlik aralar ile 5 gün ^{18}F-FDG enjekte edilerek PET/BT ile görüntülendi. ^{18}F-FDG'nin maksimum standart uptake değeri (SUV_{maks}) hesaplandı.

Bulgular: En yüksek aktivite tutulumu apse oluşumunun ilk gününde görüldü. İlk gün *S. aureus* için SUV_{maks} 3,9±0,9 iken steril apse için SUV_{maks} 2,2±0,8 idi. ^{18}F-FDG tutulumu günden güne azalırken dördüncü ve beşinci günlerde zemin aktivite düzeyi kadar azaldı. *S. aureus* ile steril apse arasında ve steril apse ile background aktivite arasında SUV_{maks} değerleri açısından ilk üç gün görüntülerde istatistiksel olarak anlamlı fark vardı ($p<0,05$). Dördüncü ve beşinci günlerde ise *S. aureus* ile steril apse arasında ve steril apse ile kontrol arasında istatistiksel olarak anlamlı bir fark yoktu ($p>0,05$).

Sonuç: Bu sonuçlar ^{18}F-FDG SUV_{maks} değerlerinin erken dönemde steril ve enfekte apse arasındaki ayrım için yararlı olabileceğini öne sürmektedir. Ayrıca ekipmanların ve işaretli ajanların lokal olarak temin edilmesi enfeksiyon enflamasyon ayrımında ^{18}F-FDG-PET görüntüleme yönteminin hızlı tanı yöntemi olmasını sağlar.

Anahtar kelimeler: Apse, enfeksiyon, enflamasyon, *S. aureus*, terebentin, pozitron emisyon tomografisi/bilgisayarlı tomografi, ^{18}F-2'-deoksi-2-fluoro-d-glukoz, sıçan

Introduction

Detecting the presence and identifying the localization of infection and inflammation have primary importance for implementation of proper treatment and patient follow-up (1,2,3,4,5,6,7). Nuclear medicine offers powerful non-invasive imaging techniques for visualization of infection and inflammation-related disorders by imaging the whole body, thus enabling determination of both the localization and extent of inflammatory foci (8,9). Various methods have been developed that display different stages of the inflammatory response. Many radiopharmaceuticals have been evaluated extensively in both preclinical and clinical studies as potential diagnostic agents to identify the sites of infection (10,11,12,13). Although there are several imaging agents, only a few of them are being used in routine clinical practice. There is a definite role of ^{18}F-2'-deoxy-2-fluoro-d-glucose (^{18}F-FDG) in assessing disease extent, disease activity in patients with infection and inflammation, and evaluation of response to treatment (6,14). The high tissue radioactivity after administration of ^{18}F-FDG corresponds to increased glucose uptake and consumption through the hexose monophosphate shunt, which is the main source of energy for chemotaxis and phagocytosis (7,15). ^{18}F-FDG, an analog of glucose, is taken up by living cells via cell membrane glucose transporters and subsequently it is phosphorylated with hexokinase inside most cells. Activation of phagocytes, also known as respiratory burst activation, lead to increased ^{18}F-FDG uptake (10). In sterile inflammation, administered ^{18}F-FDG is mainly taken up by neutrophils and macrophages (6,15). A high degree of ^{18}F-FDG uptake is detected in neutrophils during the acute phase of inflammation, while macrophages and polymorphonuclear leukocytes uptake ^{18}F-FDG during the chronic phase (1,6,11,16). ^{18}F-FDG is phagocytized by macrophages and phagocytic cells via d-glucose transporter. Through glycolysis, ^{18}F-FDG is phosphorylated by hexokinase resulting in ^{18}F-FDG-6 phosphate. Positron emission tomography (PET) imaging can be used alone or in conjunction with computed tomography (CT) in diagnosing and management of therapy planning in a variety of disorders (9).

The use of PET/CT represents the new generation in diagnostic modality. PET imaging detects an increase in metabolic activity while CT provides anatomic correlation (15,16,17,18). Inflammatory cells have an increased positive expression of glucose transporters and growth factors, which affect the affinity of these transporters for deoxyglucose. Due to structural analogy, 2-deoxyglucose ^{18}F-FDG is uptaken at the site of infection at a high level depending on the rate of glycolysis. ^{18}F-FDG is carried into the cells by the glucose transporters. In case of infection and inflammation, leukocyte activation occurs and glucose is used in the activation as an energy source. Glucose transporter receptors are stimulated by uptake of glucose and its analogues (17,19).

The aim of this study is to evaluate the development of infection and inflammation, as well as to monitor sterile and infected abscesses in rats by using ^{18}F-FDG-PET/CT.

Materials and Methods

All animals were treated in accordance with the protocols approved by the Animal Care and Use Committee of the University. The designed study was conducted at the animal care facility of the Faculty of Medicine, Dokuz Eylül University.

In this study, sterile abscess was induced by using turpentine and infected abscess was induced by using *Staphylococcus aureus* ATCC 25923 strain on rats. Three groups of rats were used for imaging as sterile, infected, and control groups. Another group of rats were used to remove the abscess tissue to compare number of living organism with standard uptake value (SUV). They were male White Wistar Rats, clinically healthy animals of 150-220 gr body weight.

Bacterial Strain and Rat Model for Abscess Formation

S. aureus strain (ATCC 25923) was grown in 5-10% sheep blood agar (Salubris, USA) after incubating overnight at 37°C.

One loop of the *S. aureus* colonies was suspended in Mueller Hinton broth (mhb) containing tube to obtain l0^7 colony-forming units (CFU)/mL.

The animals were anesthetized by intraperitoneal administration of xylazine, 5 mg/kg and ketamin, 35 mg/kg. For infected abscess formation on rats (n=14), *S. aureus* 0.5 mL 10^7 CFU/mL was inoculated in the right arm of the rats subcutaneously. For sterile abscess formation on rats (n=7) 0.2-0.4 mL turpentine (Sigma-Aldrich) was injected into the right arm of the rats subcutaneously. In the control group (n=6), 0.5 mL 0.9% NaCl was injected into the right arm of the rats subcutaneously. Following each imaging, an abscess of a rat was removed in the another *S. aureus* group and living bacterial organisms were counted in the excised tissue.

Positron Emission Tomography/Computed Tomography Imaging of Rats

A preliminary study was performed to optimize imaging time depending on abscess formation. First day image was acquired 24 hours after inoculation of *S. aureus* and turpentine. ^{18}F-FDG (37 MBq) was injected intravenously via the tail vein. Prior to ^{18}F-FDG injection, rats fasted for 4 hours and were well hydrated. Imaging was performed using PET/CT (PHILIPS Gemini TF), beginning one hour after injection of ^{18}F-FDG on the first day for five days with an interval of twenty-four hours. ^{18}F-FDG rat imaging was done with two-minute bed positions. On the first day, imaging was performed at the first and second hours after injection of ^{18}F-FDG to obtain optimum imaging time. Non-diagnostic CT images were obtained (90 kVp and 30 mAs, with a thickness slice of 2 mm, the rotation time was 0.5 sec, 39 mm/sec bed speed, 512x512 matrix).

Image Analysis

PET/CT images were visually and semi-quantitatively assessed. For semi-quantitative analysis of the PET images, a region of interest (ROI) was drawn around the abscess area on the right arm. In the control group, a ROI was drawn around a similar area as the background on the right arm. SUV_{max} was obtained from the images for evaluation of glucose metabolism of infection and inflammation detected by ^{18}F-FDG-PET/CT.

The SUV_{max} of ^{18}F-FDG uptake were calculated on abscess sites by using the formula:

SUV=Tissue concentration (Bq/g)/[injected dose (Bq)/body weight (g)]

Results

Twenty-four hours after inoculation of *S. aureus* or turpentine, swelling was apparent in the abscess site. A soft tissue infection developed on the right arm within twenty-four hours after bacterial inoculation. Swelling and redness of the abscess area were apparent in all rats. Abscess sites were visualized by ^{18}F-FDG-PET/CT. A higher abscess/background ratio was detected at the first hour compared to the second hour after injection of ^{18}F-FDG. Imaging time was chosen as the first post injection hour for the following days.

The initial SUV_{max} for *S. aureus* was 3.9±0.9 on the first day, while it was 2.2±0.8 for sterile abscess and 1.2±0.5 for control group rats. The first day SUV_{max} on the second hour following ^{18}F-FDG injection was 2.8±0.6 for infected abscess, 1.9±0.9 for sterile abscess, and 1.2±0.09 for control group. During the following two days, although activity involvement decreased at *S. aureus* it was still higher than involvement in turpentine abscess. There were statistically significant differences between *S. aureus* and sterile abscess, and between sterile abscess and control group as SUV_{max} for the first three days ($p<0.05$). On the fourth and fifth days, there was no statistically significant difference between *S. aureus* and sterile abscess, and between sterile abscess and control group ($p>0.05$).

It was observed that SUV_{max} of infected abscess was higher than that of sterile abscess in all images during the first three days. CFUs per milliliters (CFU/mL) in excised abscess tissue was 10^4 CFU/mL, 10^3 CFU/mL, 10^2 CFU/mL in the first, second and third days, respectively. There was no living organism at the fourth and fifth days. A correlation was detected between ^{18}F-FDG activity and number of living microorganisms in excised abscess tissue.

Figures 1a, 1b, 2a, 2b display ^{18}F-FDG images of sterile and infected abscess in rats.

Table 1 presents SUV_{max} for sterile abscess, infected abscess, and control rats as well as the quantity of living organisms.

Discussion

It is clinically important to distinguish infection from inflammation (6,14). Abscess is a life threatening and important complication of inflammation or major surgery (19,17). Most infectious and inflammatory foci can be visualized accurately with radiolabeled autologous leukocytes. *In vitro* labeled leukocyte imaging is the gold standard for imaging most infection. However, preparation of this radiopharmaceutical is laborious, time consuming and requires handling of potentially contaminated blood (4). New agents are being developed that could potentially differentiate between infection and non-microbial inflammation. In addition to these, it is suggested that ^{18}F-FDG-PET imaging can be used to visualize inflammatory foci when a high spatial resolution is required (1).

Kumar et al. (20) compared ^{67}Ga Citrate SPECT and ^{68}Ga Citrate PET in *S. aureus* infection in the rat model. They concluded that ^{68}Ga Citrate PET is a faster imaging method

as ^{68}Ga has a half-life of 68 minutes compared to 78.3 hours for ^{67}Ga. Yamada et al. (21) studied ^{18}F-FDG uptake and its distribution in turpentine induced inflammatory tissue on male Donryu rats. They showed that the uptake in inflammatory tissue increased gradually upto 60 minutes and then decreased. Our study also showed an increased activity within 60 minutes followed by a decreased activity 120 minutes after injection of ^{18}F-FDG. They reported an increasing activity which peaked on the 4 day after inoculation followed by a slow down. Our study detected the highest ^{18}F-FDG activity a day after turpentine inoculation. In our study, there was also a correlation between ^{18}F-FDG activity and quantity of living microorganisms in excised abscess tissue. These differences may be due to the rat's immune tolerance.

Kaim et al. (22) studied ^{18}F-FDG and ^{18}F-FET in an acute phase abscess model. Their histological study showed increased ^{18}F-FDG uptake that corresponded to cellular inflammatory infiltrates, mainly consisting of granulocytes. The necrotic abscess center and the second necrotic tissue layer were characterized by decreased ^{18}F-FDG uptake. They documented a marked increase in ^{18}F-FDG uptake at the site of infection, which could be attributed to activated granulocytes and macrophages. In their study, ^{18}F-FET uptake was low in inflammatory infiltrates consisting of neutrophil, granulocytes and macrophages. They interpreted this finding as either low uptake in the bacterial area may be lacking bacterial uptake by ^{18}F-FET or small number of living bacteria in the infection area. On the other hand, our study demonstrated that there was a correlation between bacterial load and ^{18}F-FDG uptake rate. A greater bacterial load in the excised abscess yielded a higher SUV.

Sugawara et al. (23) compared ^{18}F-FDG, thymidine, L-methionine, ^{67}Ga Citrate and ^{125}I-HSA in sites of bacterial infection in rats infected with *E. coli*. Their auto-radiographic study detected the highest ^{18}F-FDG uptake in the inflammatory area of cell infiltration surrounding the necrotic region. In their study, ^{18}F-FDG showed much higher uptake values than ^{67}Ga Citrate or ^{125}I-HSA. They reported lower methionine and thymidine accumulation in the infectious foci than ^{18}F-FDG. In their bacterial model, an abscess was formed and the necrotic area showed slightly higher ^{18}F-FDG uptake than the surrounding edematous muscle, while the center of the abscess in turpentine model showed very low ^{18}F-FDG uptake. In our study, ^{18}F-FDG uptake in the bacterial site was higher than the inflammation site. It has been reported that abscess-forming bacteria utilize glucose as an energy source using various pathways. The lack of any ^{18}F-FDG uptake could be attributed to a low number of inflammatory cells, lack of granulation tissue, or absence of microorganisms.

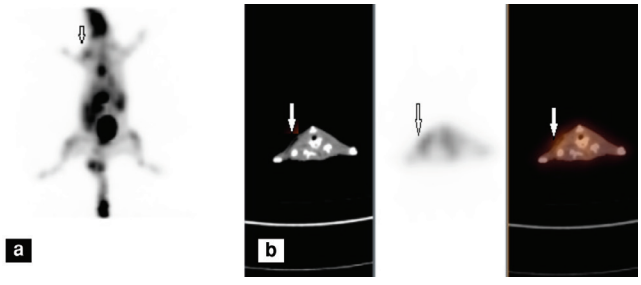

Figure 1. Sterile abscess imaging in rats by using ^{18}F-2'-deoxy-2-fluoro-d-glucose positron emission tomography/computed tomography, (a) 3D MIP image, (b) Transverse cross-sectional images, computed tomography, positron emission tomography and fusion images

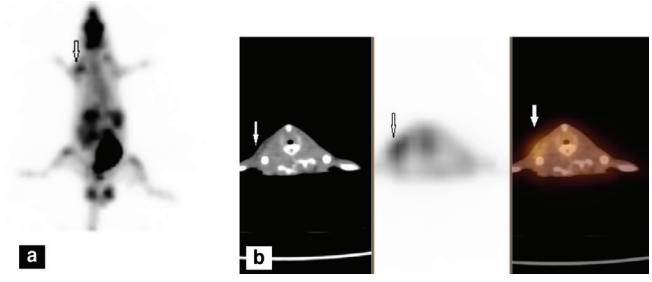

Figure 2. Infected abscess imaging in rats by using ^{18}F-2'-deoxy-2-fluoro-d-glucose positron emission tomography/computed tomography, (a) 3D MIP image, (b) Transverse cross-sectional images, computed tomography, positron emission tomography and fusion images

Table 1. Maximum standard uptake values for sterile abscess, infected abscess and control and number of living organism

	SUV_{max}			
Imaging times	**Infected abscess**	**Sterile abscess**	**Control**	**Living organism CFU/mL**
First day at one hour	3.9±0.9	2.2±0.8	1.2±0.5	$1x10^4$
First day at two hour	2.8±0.6	1.9±0.9	1.2±0.3	
Second day at one hour	1.9±0.2	1.8 ±1	0.9±0.3	$1x10^3$
Third day at one hour	1.2±0.4	0.9±0.3	0.7±0.2	$1x10^2$
Fourt day at one hour	0.9±0.5	0.7±0.3	0.7±0.3	No living organism
Fifth day at one hour	0.8±0.4	0.7±0.2	0.7±0.2	No living organism

CFU: Colony-forming units, Suv_{max}: Maximum standard uptake

Dumarey et al. (24) used ^{18}F-FDG labeled leukocytes for imaging of inflammation. They found high sensitivity and specificity rates for the diagnosis of infection. They concluded that due to ^{18}F-FDG uptake in the brain, the genitourinary tract and variable activity in the myocardium, bone marrow, stomach and bowel, ^{18}F-FDG-PET had poorer diagnostic performance compared with labeled leukocytes for the detection of infection in these sites. We also observed major uptake in these organs. We agree with Dumarey et al. (24) that the diagnostic performance of ^{18}F-FDG imaging in infection of these sites is poor. However, leukocyte labeling procedure is time consuming and needs careful handling process.

Pellegrino et al. (25) carried out a study to compare the relative uptakes of ^{18}F-FDG and of ^{18}F-FDG labeled WBCs in sterile and septic inflammation foci in an animal model. Their results showed that ^{18}F-FDG-WBC PET imaging had a greater performance versus ^{18}F-FDG in the sterile inflammation model as well as in *E.coli* and *P. aeruginosa* septic models. Jamar et al. (26) emphasized that it should be kept in mind that the choice between ^{18}F-FDG imaging and an alternative technique depends on the need for rapid diagnosis and local availability of required equipment and labeled agents.

In our study, the highest ^{18}F-FDG activity was observed on the first day following inoculation in the infection and the inflammation sites, and then the activity decreased day by day. This could be related to the rapid metabolic activity in fast recovering rats. On the fourth and fifth days, ^{18}F-FDG activity was equal to that of the controls. We compared activity rates according to bacterial load by excising tissue. It was seen that bacterial load and ^{18}F-FDG uptake values correlated with infection severity. In this study, the imaging was performed by PET/CT that is designed for human body imaging, if imaging studies had been obtained with small animal imaging device (microPET/CT) resolution of the images would have been higher than the presented images.

Conclusion

Inflammatory and infected tissues utilize glucose as energy source for chemotaxis and phagocytosis. Therefore, the accumulation of ^{18}F-FDG as a glucose analog can be used for diagnosis of infection and inflammation. Sterile and infected abscess differentiation can be evaluated by imaging with ^{18}F-FDG-PET at early phase. The value of SUV_{max} explores correlation between sterile abscess and infected abscess. ^{18}F-FDG-PET is also a useful technique to understand the extent of the infection and inflammation process. In addition to PET imaging method with ^{18}F-FDG has the possibility of rapid diagnosis and easier with the advantage of local availability.

Ethics

Ethics Committee Approval and Informed Consent: All animals were treated in accordance with the protocols approved by the Animal Care and Use Committee of the University. The designed study was conducted at the animal care facility of the Faculty of Medicine, Dokuz Eylül University.

Peer-review: Externally peer-reviewed.

Authorship Contributions

Surgical and Medical Practices: T.E., M.S.E., M.K., G.O., H.D., Concept: T.E., M.S.E., M.K., G.O., H.D., Design: T.E., M.S.E., M.K., G.O., H.D., Data Collection or Processing: T.E., M.S.E., M.K., G.O., H.D., Analysis or Interpretation: T.E., M.S.E., M.K., G.O., H.D., Literature Search: T.E., M.S.E., M.K., G.O., H.D., Writing: T.E., M.S.E., M.K., G.O., H.D.

Conflict of Interest: No conflict of interest was declared by the authors.

Financial Disclosure: The authors declared that this study received no financial support.

References

1. Kumar R, Basu S, Torigian D, Anand V, Zhuang H, Alavi A. Role of modern imaging techniques for diagnosis of infection in the era of 18F-Fluorodeoxyglucose positron emission tomography. Clin Microbiol Rev 2008;21:209-224.
2. Gotthardt M, Bleeker-Rovers CP, Boerman OC, Oyen WJG. Imaging of inflammation by PET, conventional scintigraphy, and other imaging techniques. J Nucl Med 2010;51:1937-1949.
3. Petruzzi, N, Shanthly N, Thakur M. Recent Trends in Soft Tissue Infection Imaging. Semin Nucl Med 2009;39:115-123.
4. Vangu MW. Infection imaging in nuclear medicine Nuclear medicine has a role to play in investigating patients with suspected infection. CME 2013;31:295.
5. Mahfouz T, Miceli MH, Saghafifar F, Stroud S, Jones-Jackson L, Walker R, Grazziutti ML, Purnell G, Fassas A, Tricot G, Barlogie B, Anaissie E, 18F-Fluorodeoxyglucose positron emission tomography contributes to the diagnosis and management of infections in patients with multiple myeloma: a study of 165 infectious episodes. J Clin Oncol 2005;23:7857-7863.
6. Kumar R, RN Murali, Balakrishnan V, Bal C, Malhotra A. FDG-PET imaging in infection and inflammation. IJNM 2006;21:104-113.
7. Elgazzar AH, Elmonayeri M. The pathophysiologic basis of nuclear medicine. Elgazzar AH (ed). Inflammation. Newyork, Springer-Verlag Berlin Heidelberg, 2006;67-89.
8. Bleeker-Rovers CP, Boerman OC, Oyen WJH. Radiolabeled compounds in diagnosis of infectious and inflammatory disease. Curr Pharm Des 2004;10:2935-2950.
9. Love C, Palestro CJ. Radionuclide imaging of infection. J Nucl Med Technol 2004;32:47-57.
10. Goldsmith SJ, Vallabhajosula S. Clinically Proven Radiopharmaceuticals For Infection Imaging: Mechanisms And Applications. Semin Nucl Med 2009;39:2-10.
11. Truluck CA. Inflammation and infection imaging, nuclear medicine technology. J Radiol Nurs 2007;26:77-85.
12. Laverman P, Bleeker-Rovers CP, Corstens FHM, Boerman OC, Oyen WJG. Development of Infection and Inflammation Targeting Compounds Current. Radiopharmaceuticals 2008;1:42-48.
13. Welling M, Feitsma HJ, Calume W, Pauwels EKJ. Detection of experimental infections with 99mtc-Labeled Monoclonal Antibodies Against Tnf-(X And Interleukin-8). Nucl Med Biol 1997;24:649-655.
14. Glaudemans AW, de Vries EF, Galli F, Dierckx RA, Slart RH, Signore A. The Use of 18F-FDG-PET/CT for diagnosis and treatment monitoring of inflammatory and infectious diseases. Clin Dev Immunol 2013;2013:623036.

15. Burt BM, Hummy JL, Kooby DA, Squirey OD, Mastoridesz S, Larsony SM, Fong Y. Using positron emission tomography with [18F]FDG to predict tumor behavior in experimental colorectal cancer. Neoplasia 2001;3:189-195.
16. A Vera. FDG-PET/CT in the detection of infections and inflammations. Arch Oncol 2012;20:103-106.
17. Rudd JHF, Narula J, Strauss HW, Virmani R, Machac J, Klimas M, Tahara N, Fuster V, Warburton EA, Fayad ZA, Tawakol AA. Imaging atherosclerotic plaque inflammation by fluorodeoxyglucose with positron emission tomography. J Am Coll Cardiol 2010;55:2527-2535.
18. Coker CO. Flurodeoxyglucose positron emission tomography: a new technique to evaluate infectious processes. Chapter 2008;42:217-220.
19. Sabah S. Imaging infection and inflammation in children with 18F-FDG-PET and 18F-FDG-PET/CT. J Nucl Med Technol 2011;39:179-182.
20. Kumar V, Boddeti DK, Evans SG, Angelides S. 68Ga-Citrate-PET for diagnostic imaging of infection in rats and for intra-abdominal infection in a patient. Curr Radiopharm 2012;5:71-75.
21. Yamada S, Kubota K, Kubota R, Ido T, Tamahashi N. High accumulation of fluorine-18-fluorodeoxyglucose in turpentine-induced inflammatory tissue. J Nucl Med 1995;36:1301-1306.
22. Kaim AH, Weber B, Kurrer MO, Westera G, Schweitzer A, Gottschalk J, Von Schulthess GK, Buck A. 18F-FDG and 18F-FET uptake in experimental soft tissue infection. Eur J Nucl Med 2002;29:648-654.
23. Sugawara Y, Gutowski TD, Fisher SJ, Brown RS, Wahl RL. Uptake of positron emission tomography tracers in experimental bacterial infections: a comparative biodistribution study of radiolabeled FDG, thymidine, L-methionine, 67Ga-citrate, and 125I-HSA. Eur J Nucl Med 1999;26:333-341.
24. Dumarey N, Egrise D, Blocklet D, Stallenberg B, Remmelink M, Marmol V, Simaeys GV, Jacobs F, Goldman S. Imaging infection with 18 F-FDG-labeled leukocyte PET/CT: initial experience in 21 patients. J Nucl Med 2006;47:625-632.
25. Pellegrino D, Bonab AA, Dragotakes SC, Pitman JT, Mariani G, Carter EA. Inflammation and infection: imaging properties of 18F-FDG-labeled white blood cells versus 18F-FDG. J Nucl Med 2005;46:1522-1530.
26. Jamar F, Buscombe J, Chiti A, Christian PE, Delbeke D, Donohoe KJ, Israel O, Martin-Comin J, Signore A. EANM/SNMMI Guideline for 18F-FDG use in inflammation and infection. J Nucl Med 2013;54:647-658.

Original Article
Mol Imaging Radionucl Ther 2017;26:53-61 DOI:10.4274/mirt.30932

Experimental and Simulation Analysis of Radiation of the Beta Emitting Sources in a Magnetic Field

Manyetik Alanda Beta Yayan Kaynakların Işınımının Deneysel ve Simülasyon Analizi

Berrin Çavuşoğlu[1], Selda Sucu[1], Hatice Durak[2], Kadir Akgüngör[3], Hakan Epik[3], Türkan Ertay[2]
[1]Dokuz Eylül University Health Sciences Institute, Department of Medical Physics, İzmir, Turkey
[2]Dokuz Eylül University Faculty of Medicine, Department of Nuclear Medicine, İzmir, Turkey
[3]Dokuz Eylül University Faculty of Sciences, Department of Physics, İzmir, Turkey

Abstract

Objective: The behavior of beta particles under the magnetic field was investigated both theoretically and experimentally based on the assumption of reducing the damage to the normal tissues created by using magnetic field in radionuclide therapy.

Methods: A water-filled spherical medium and a beta particle source was formed by using Geant4 simulation software for the theoretical study. After applying a homogenous magnetic field, the volume of points at which the particles interact with the medium was calculated by determining particle range. The range of beta particles was examined using yttrium-90 source and Gafchromic films for the experimental study. The setup was kept in normal room conditions and in the magnetic resonance imaging device. Then the irradiated films were analyzed by creating isodose curves.

Results: With the increase of the magnetic field, the number of hits at the center was increased, but the number of hits at the outer boundaries decreased inversely proportional to the strength of the magnetic field. The change perpendicular to the magnetic field was greater as compared to the change parallel to the magnetic field. The volume of hits of beta particles got smaller with the increase of the magnetic field.

Conclusion: When magnetic field is increased, the decrease in the number of interactions at the outer boundaries became more pronounced in the perpendicular direction to the magnetic field. The effect of magnetic field was more apparent for higher energy beta particles than lower energy particles.

Keywords: Beta radiation, magnetic field, Geant4 Monte Carlo simulation, yttrium-90

Öz

Amaç: Beta yayan radyoizotoplarla yapılan kanser tedavilerinde manyetik alan kullanılarak normal dokularda oluşan zararın azaltılmasının mümkün olabileceği varsayımı ile beta parçacıklarının manyetik alandaki davranışları teorik ve deneysel olarak araştırıldı.

Yöntem: Teorik çalışmada, Geant4 programında içi su dolu küresel bir ortam oluşturuldu ve merkezine beta parçacığı kaynağı yerleştirildi. Homojen bir manyetik alan uygulanarak parçacıkların ortamla etkileştikleri noktaların hacmi, parçacıklarının menzilleri belirlenerek hesaplandı. Deneysel çalışmada, beta parçacıklarının menzili itriyum-90 kaynağı ve Gafkromik film kullanılarak incelendi. Düzenek normal oda koşullarında ve manyetik rezonans görüntüleme cihazında bekletildi. Işınlanan filmler izodoz eğrileri oluşturularak analiz edildi.

Address for Correspondence: Berrin Çavuşoğlu PhD, Dokuz Eylül University Health Sciences Institute, Department of Medical Physics, İzmir, Turkey
Phone: +90 232 412 35 93 E-mail: berrncavusoglu@gmail.com **Received:** 23.03.2016 **Accepted:** 16.02.2017

Öz

Bulgular: Manyetik alan artmasıyla beraber merkezde etkileşim sayısında artma olduğu, merkezin dışında ise etkileşim sayısının manyetik alanla ters orantılı olarak azaldığı görüldü. Manyetik alana dik yöndeki değişim manyetik alana paralel yöndekine göre daha fazla idi. Manyetik alanın artmasıyla beta parçacıklarının etkileştiği hacim küçülmekte idi.

Sonuç: Manyetik alan arttıkça, manyetik alana dik yönlerde merkezin dışındaki alanlarda etkileşim sayısındaki azalım daha belirgin olmaktadır. Manyetik alan etkisinin düşük enerjililere oranla yüksek enerjili beta parçacıklarında daha belirgin olduğu görülmüştür.

Anahtar kelimeler: Beta radyasyonu, manyetik alan, Geant4 Monte Carlo simülasyonu, itriyum-90

Introduction

Radionuclide therapy utilizes ionizing radiation for the treatment of undesired tissues such as tumors or an over active thyroid gland. For this purpose, radiation dose is given to the target tissue using radionuclides emitting β-, a+ or Auger electrons. Beta emitters are locally used in prostate seed implants and coronary artery stents, or are systemically administered for the treatment of bone metastases, ablation of thyroid tissue, radioimmunotherapy, etc (1).

Beta particles lose their energy like other charged particles through ionization and cause excitation in soft tissue or water (2). They deviate from their paths as a result of their interaction with atomic nuclei and electrons on their way, depending on the type of medium and the energy of the beta particle (3).

In smaller tumors, the range of beta particles may be greater than the lesion size and only some of their energy accumulates in target cells. Thus, the remaining energy of the ionizing radiation administered may cause damage to normal cells since the surrounding healthy cells cannot be protected and the energy is absorbed by healthy cells as well (1).

The damage to healthy cells causes undesirable side-effects due to the long range of beta particles. The application of a strong magnetic field has been suggested for reducing the particle range in a wide variety of applications of beta radiation. The charged particle entering the magnetic field traces circular paths with the effect of magnetic force (4). Considering the change in the paths of charged particles in the magnetic field, it may be possible to prevent beta particles to leave the target tissue, thus reducing the side effects and increasing the dose to the center, which in turn would increase therapeutic effectiveness. This effect of the magnetic field has been shown in a few studies to enhance the radiation dose absorbed by tumors (5,6) and to protect bone marrow (7).

The theoretical study of the change in the paths of beta particles can be performed by using a computer simulation. In this study, we simulated the course of the interaction of beta particles with matter in magnetic field using Geant4. Geant4 is a Monte Carlo-based particle simulation program developed at CERN, which models and simulates the interaction of different particles within matter (8).

The main goal of this approach was to seek a means of reducing the damage to normal cells during nuclear medicine procedures. For this reason, in this study, the movements of beta particles in magnetic field were investigated with the assumption that it is possible to change both the irradiated volume and the dose by using magnetic field in radionuclide therapy.

Materials and Methods

Simulation

The geometrical dose distribution of beta (β-) radiation with 0.5-2 MeV energy from a point source in a medium, with different magnetic field strengths (0-3 T) was simulated and analyzed.

Initially, a water-filled spherical medium with a radius of 1.5 cm in which radiation will be detected was created for the simulation. Then a particle source was placed at the center where the beta particles will be thrown mono energetically in random directions. Physical processes and type of interaction of the particles with matter within the medium were determined and included in the simulation. Geometrically homogenous magnetic field was applied in x-direction and then y-axis was chosen to assess the effect of magnetic field on the range of the particles.

To obtain various data including as the positions and energies of the beta particles, slices of 0.1 mm thickness were formed on y-axis so as to be separated 1.0 mm from each other.

Information about the particle at different coordinates where it interacts with the medium was written on text files for each slice. The simulation was done for 10^6 beta particles with the energies of 0.5, 1, 1.5 and 2 MeV at different magnetic fields, namely 0, 0.5, 1, 1.5, 2, 2.5 and 3 T.

The data including interactions, positions and energies of each slice were recorded from the simulation program Geant4. To analyze the data, each slice was divided into stripes of 0.5 mm apart in both directions, perpendicular (z-axis) and parallel (x-axis) to the magnetic field.

By counting the number of hits in each stripe, we were able to know the change in the amount of interactions starting from the center of the source and also the shape of the interaction volume.

These analyses were done for all the above-mentioned beta energies and magnetic fields.

With these analyses, we measured the dimensions of the volume consisting of the hit points with the medium. The volume was considered to be an ellipsoid and the dimensions were calculated by determining the ranges of particles on each axis. Then the change in the volume of interaction was compared for each energy level and different magnetic fields. This simulation study was approved by the local ethical committee (122/2009).

Experiment

We used high energy beta (β-) emitter yttrium-90 (^{90}Y) glass microspheres to assess the effect of magnetic field on the range of beta particles. ^{90}Y decays by beta emission with end-point energy of 2.28 MeV with a mean of 0.93 MeV and a half-life of 64.1 h (9). The maximum range of the ^{90}Y beta radiation in water is 11 mm with a mean of 2.5 mm (10).

The range of beta particles was examined using Gafchromic EBT (Beam Therapy) films. Gafchromic EBT radiachromic film dosimeters are used to measure absorbed dose as a function of position in the phantom with a dose range of 2-800 cGy. When exposed to radiation, the color changes by photoionization from colorless to deep blue as a function of absorbed dose (11,12,13).

1.5 T Philips Achieva magnetic resonance imaging (MRI) scanner (Philips Medical Systems, Best, The Netherlands) was used as the source for high magnetic field.

The experimental setup was made of plexiglas. 6.4 mCi ^{90}Y radioactive source was put into a capillary tube and the lower end of the tube was used as a point source. The radiochromic film was cut into small pieces and put into setup as perpendicular to the capillary tube. Then the setup was placed in water filled container. The first film was exposed for 1 hour, and then the number of decays was calculated as 4.25×10^{11}. Each film was kept in normal room conditions and exposed to the same number of decays (4.25×10^{11}) without magnetic field (0 T) or in the MRI scanner (1.5 T). The experiment was performed at 0 T and 1.5 T for different distances between the source and the film (0 mm and 2 mm) and repeated four times for each. The irradiated films were analyzed using Matlab Image Processing Toolbox by creating isodose curves (Figure 1). The diameters of isodose curves were measured on each axis, parallel (x-axis) and perpendicular (y-axis) to the magnetic field, to calculate the amount of reduction in irradiated areas at magnetic field. This experimental study was approved by the Dokuz Eylül University Local Ethical Committee (121/2009).

Results

Geant4 Simulation

Simulation revealed that the beta particles stayed closer to the source due to the magnetic force as the magnetic field increased, thus the interaction range was reduced (Figure 2, 3).

The paths of a few representative 2 MeV beta particles in different magnetic fields in x-direction are shown in Figure 4. It is seen that the beta particles are localized to the center as the magnetic field increased.

Beta particles changed their directions and moved towards the x-axis under the magnetic field. With the increase of the magnetic field, ranges of the particles were perpendicularly shortened.

The hit numbers of beta particles with 0.5, 1, 1.5, 2 MeV energies in different slices were calculated. To represent

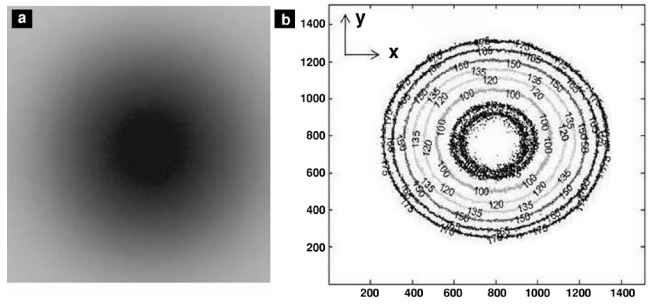

Figure 1. The images of (a) an irradiated film and (b) the isodose curves created by Matlab are shown as an example. The magnetic field is applied on x-axis

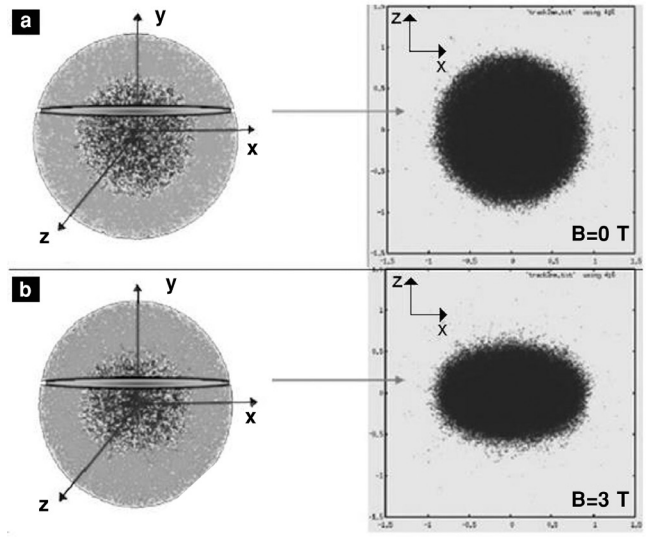

Figure 2. The 3D simulation images of water medium by 10^6 beta particles with 2 MeV energy from the point source and the images of 2D slices on xz-plane, (a) without magnetic field and (b) with 3 T magnetic field. The shown example slices are taken 2 mm from the center

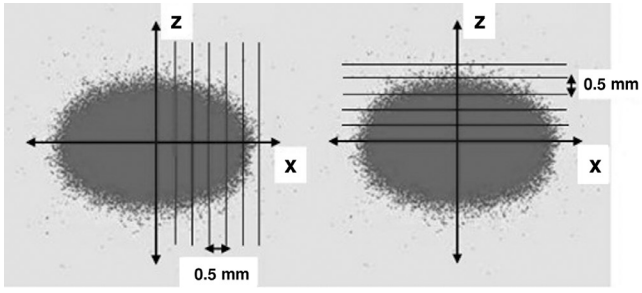

Figure 3. The calculation of hit numbers with 0.5 mm distances along the x-axis (on the left hand side) and the z-axis (on the right hand side) for analyzing the data obtained from Geant4 program

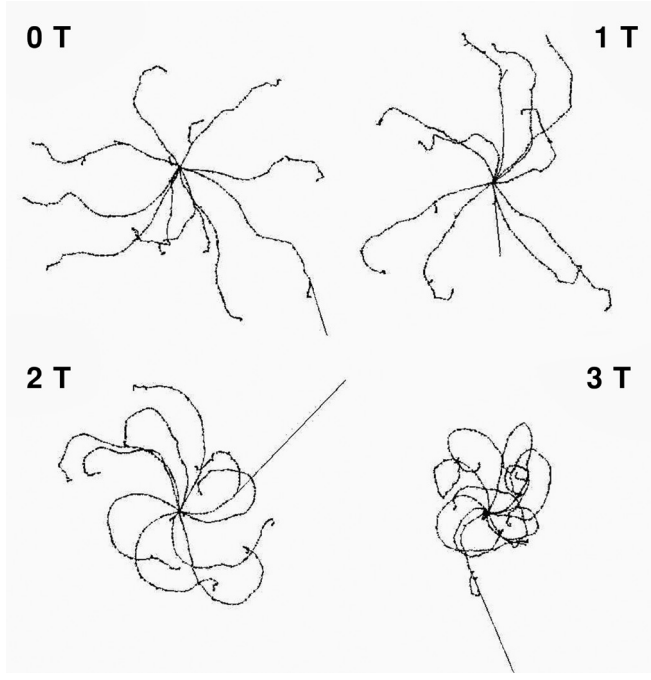

Figure 4. The 3D images of the paths followed by 10 beta particles with 2 MeV of energy from the source in 0 T, 1 T, 2 T, 3 T magnetic fields are shown as an example of the simulation. The magnetic field is applied perpendicular to the page

the results, only 2 MeV energy beta particles at different magnetic fields are shown (Figure 5).

In the inner slice (2 mm) from the center, the number of hits was increased on the x-axis with the amplification of the magnetic field. However, the number of hits was sharply decreased beyond 3 mm on the z-axis. Since the shape of the interaction area was elliptical, the number of hits was increased by 20% for 3 T at the center. On the other hand, the area was the same as the shape of the sphere for 0 T, as expected. Figure 5 (c) also shows that the increased magnetic field reduced the number of hits rapidly. As a result, the counts vanished at higher magnetic fields at the outmost slice.

We calculated the interaction volumes and found that they were reduced by 16% for 1 MeV, 31% for 2 MeV at 2 T relative to zero magnetic field, as seen in Table 1. It should be also noted that the reduction in the volume was much larger at higher magnetic fields. For example, it was reduced by 35% for 1 MeV and 53% for 2 MeV at 3 T. The ratio of the volumes with and without magnetic field is shown in Table 1.

As shown in Table 1, the volume got distinctly smaller as the magnetic field increased, which effect on the volume was with the increase in beta energy.

Experiment

Mean diameters of isodose curves measured on 4 irradiated films were used to assess the effect of magnetic field (Table 2, 3). Mean values of diameters were compared for 0 T and 1.5 T for each isodose curve, from 1 (innermost isodose curve) to 6 (outermost isodose curve) (Figure 6, 7).

When magnetic field was applied, the beta particles were seen to be localized to the center on x-axis (parallel to the magnetic field). The diameter of isodose curves close to the center was increased by 5%. On the other hand, the outer isodose curves were reduced by 8% on y-axis (perpendicular to the magnetic field).

As seen in Figure 7, we couldn't find any significant difference on x-axis at 2 mm distance from the source when magnetic field was applied. However, diameter of isodose curves of irradiated films was reduced by 13% under magnetic field.

Table 1. Ratio of volumes for different magnetic fields (0-3 T) for beta particles with 0.5-2 MeV energy

B (T)	0.5 MeV	1 MeV	1.5 MeV	2 MeV
0.5	0.99	0.99	0.98	0.97
1	0.99	0.95	0.94	0.91
1.5	0.98	0.90	0.84	0.85
2	0.96	0.84	0.72	0.69
2.5	0.93	0.75	0.61	0.58
3	0.91	0.65	0.52	0.47

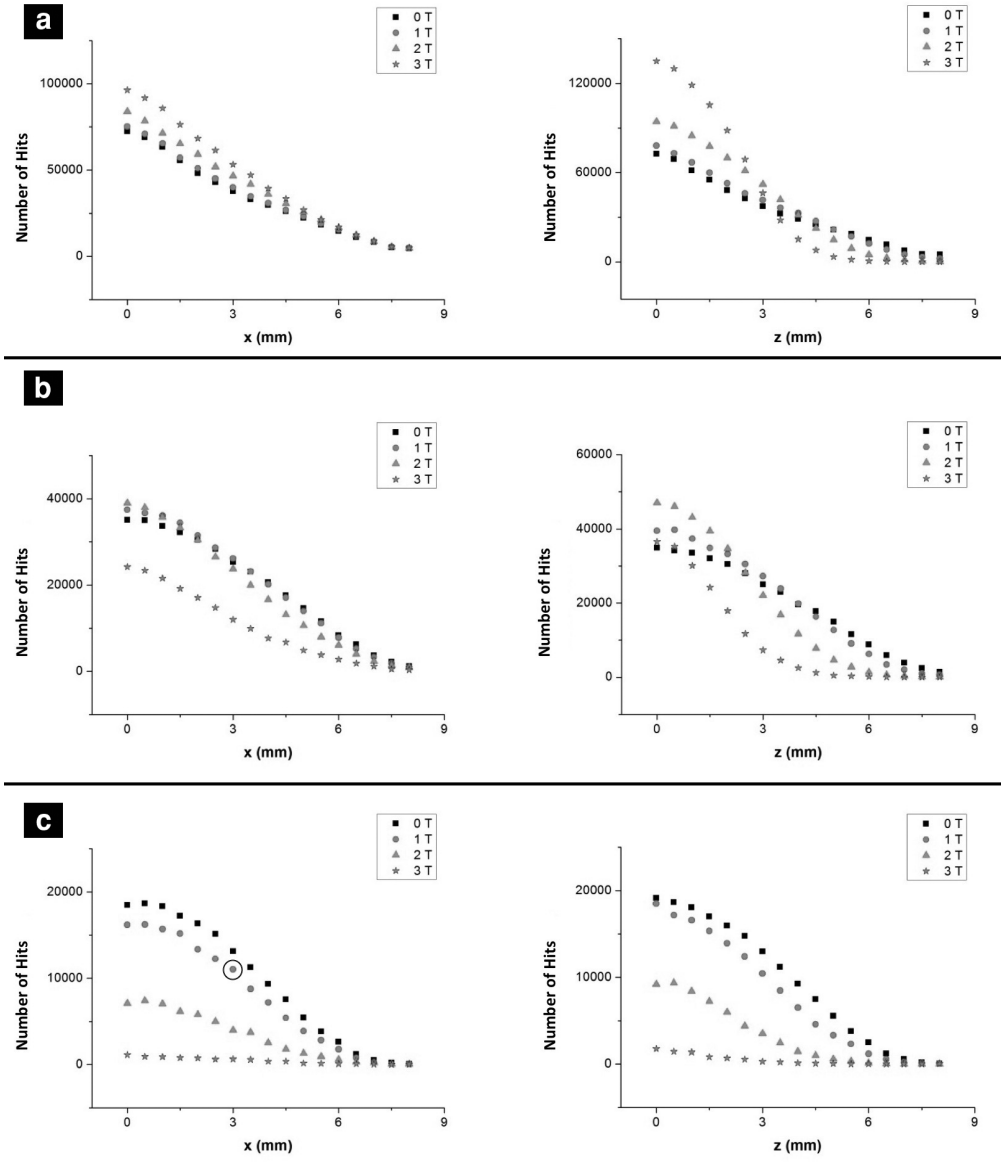

Figure 5. Number of hits of betas with 2 MeV energy under 0 T, 1 T, 2 T and 3 T magnetic fields on the x-axis of the field (on the left) and on the z-axis of the field (on the right) for the slices in (a) 2 mm (b) 4 mm (c) 6 mm from the center. In this figure each point represents the number of hits at a certain stripe of a slice

Table 2. Mean and standard deviation of diameter of isodose curves at 0 and 1.5 T for 0 mm distance from the source on x-axis (parallel to the magnetic field) and y-axis (perpendicular to the magnetic field)

		Isodose curves					
	B (T)	1	2	3	4	5	6
x	0	166.0±10.0	175.3±7.4	189.8±7.3	202.0±7.0	217.8±6.2	237.0±4.7
	1.5	179.7±9.5	190.7± 9.7	202.7±10.1	213.7±11.0	229.3±12.5	248.0±15.6
y	0	167.8±11.0	179.0±9.5	190.8±9.0	203.0±8.5	218.5±7.2	237.3±5.6
	1.5	161.0±7.5	171.0±8.5	180.7±9.0	190.7±10.0	204.0±12.0	220.3±14.5

Discussion

Ionizing radiation is widely used to treat malignant cells. Numerous novel treatments have been introduced by the internal administration of radiopharmaceuticals called targeted radionuclide therapy, in which radiolabeled molecules are specifically targeted to apply high radiation dose to the cancerous cells while striving to give minimum dose to the healthy cells through the use of the features of radiopharmaceutical uptake mechanisms (14). Radionuclide therapy is based on the use of pharmaceuticals as carriers of radionuclides to their target molecule on the surface of tumor cells. Radiation causes irreversible DNA damage and induces cell death through cross-fire irradiation (15). The main objective of the radionuclide therapy is the delivery of radionuclides to tumor cells without any risks for healthy cells (16).

The treatment response of tumors may be insufficient if the targeted lesion dose is lower than required (17). The ranges of beta particles used in these treatments can exceed the size of the target tissue, therefore causing the so called crossfire effect to surrounding cells, which is sometimes undesirable if they are healthy cells. Other problems include the heterogeneity of dose (18) and the dose limiting factors such as bone marrow toxicity (19). Because the path of beta particles changes in the magnetic field, leaving the

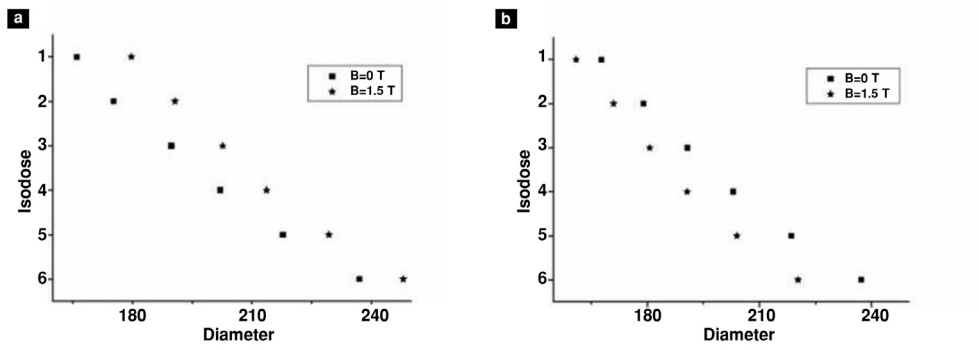

Figure 6. The graph of isodose curves on (a) x-axis and (b) y-axis at 0 T and 1.5 T for 0 mm shows that diameters of isodose curves are increased on x-axis and decreased on y-axis with the effect of the magnetic field

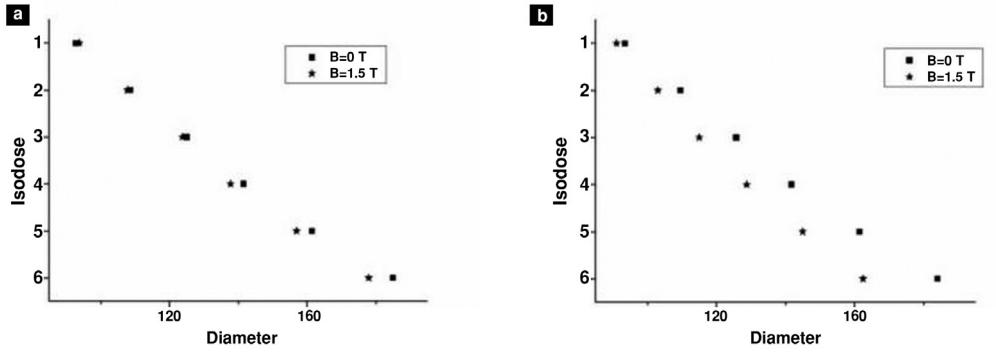

Figure 7. The graph of isodose curves on (a) x-axis and (b) y-axis at 0 T and 1.5 T for 2 mm shows that diameters of isodose curves are decreased especially on y-axis with the effect of the magnetic field

Table 3. Mean and standard deviation of diameter of isodose curves at 0 and 1.5 T for 2 mm distance from the source on x-axis (parallel to the magnetic field) and y-axis (perpendicular to the magnetic field)

		Isodose curves					
	B (T)	1	2	3	4	5	6
x	0	92.8±11.9	108.5±11.6	125.0±11.2	141.5±9.9	161.5±7.5	185.0±6.6
	1.5	93.8±17.0	107.8± 17.0	123.8±17.4	137.8±17.0	157.0±17.4	178.0±16.4
y	0	93.5±13.5	109.5±12.8	125.8±11.9	141.8±10.8	161.5±8.1	184.0±7.4
	1.5	91.0±13.6	103.0±13.4	115.0±13.7	128.8±12.9	145.0±14.1	162.5±14.3

target tissue can be prevented and it may be possible to reduce the damaging effects to the surrounding healthy tissues, while increasing the radiation effect at the center.

The application of a strong static magnetic field can be used for the benefit of nuclear medical applications. Static homogeneous magnetic field exerts a force on a charged particle and changes the paths of particles. This force, known as the Lorentz force, causes the path of charged particle to curve about the field's axis thus resulting in a helical path (20). This method has been used to increase the resolution of positron emission tomography (PET) scanners (4,21,22,23,24,25). The positron (β+) is the antiparticle of the β-, and has the same properties as the β- except its electric charge. In magnetic field, the positron moves in circular paths like the β- particle, but in opposite directions due to its opposite charge (26).

In the study carried out by Raaijmakers et al. (27), the effect of magnetic field to the dose was examined experimentally in an MRI-accelerator, and the findings were compared with the results of the Geant4 simulation. It was shown that dose effects of magnetic field can be modeled using Geant4 and that Geant4 is a suitable Monte Carlo code to study the effect of magnetic field on dose distribution for MRI-accelerator.

Wirrwar et al. (21) evaluated the potential effects of magnetic field on shortening the ranges of high energy positrons in PET. Geant simulation model was found suitable and it was reported that 4.5 T homogenous static magnetic field increased the spatial resolution in PET by reducing the high energy positron range. In another study performed by Desbrée et al. (22), the authors examined their previously developed beta microprobe in magnetic field since the combination of nuclear magnetic resonance with PET has become a current issue. The efficiency of the probe for each isotope was investigated by simulating the effect of magnetic field on the ranges of positrons with Geant4. Similarly, in this study, magnetic field shortened the ranges and decreased the volume of interaction of the positrons. In another study carried out by Christensen et al. (23), it was experimentally demonstrated that the spatial resolution in PET images was improved, because positrons were annihilated in a place closer to their point of origin in the strong magnetic field. Similar findings were reported in other simulation studies performed by Iida et al. (24), Rickey et al. (25) and Raylman et al. (4).

Raylman and Wahl (6) showed a reduction in the accumulated dose in normal tissues in radionuclide treatment using different radioisotopes at 10 T with computer simulation. In their other simulation study, they showed a decrease in the deposited bone marrow dose at 10 T during treatment of bone tumors (7). In their experimental cell culture study, they also found a reduction in the number of living lymphoma cells after irradiation at 7 T (28). They claimed that the presence of a strong magnetic field makes treatment of small tumors more effective and decreases the radiation dose to normal tissues.

In this study, we showed that when magnetic field is applied, beta particles deviated from their paths resulting in accumulation of the radiation in the center of the source with a decrease in outer boundaries. In the simulation study, we found that the reduction in the irradiated volume is much larger at higher magnetic fields with 9% at 1 T, 31% at 2 T and 53% at 3 T for 2 MeV. We also showed the effect of magnetic field experimentally. For this purpose, we set an experimental design close to the simulation. However, there were a few differences between methods, such as used sources, shape of sources, tube glass between radiation and water. For this reason, we couldn't compare the findings obtained from the two methods since absolute particle range was not calculated. However, we were able to observe the geometric distribution of the radiation in two dimensions, parallel and perpendicular to the magnetic field, like in the simulation. We experimentally showed that at the distance of 0 mm from the source, the change parallel to the magnetic field at the inner isodose curves was greater by 5% when magnetic field was applied as compared to the isodose curves of the films irradiated without magnetic field. At 2 mm distance from the source to the direction perpendicular to the magnetic field, there was a reduction of approximately 13% as compared to the change of the diameters of isodose curves of the films irradiated without magnetic field.

The shortcomings of this study include limited number of experiments due to the short half-life of ^{90}Y source. Also, we could obtain only a few data at 0 and 2 mm distance from the source because of the short range of beta particles. In addition, we could not compare the simulation findings with experimental data, as different energy sources were used in the simulation and the experimental study.

Conclusion

In this study, the magnetic field's effect on beta particles in tissue equivalent water was investigated by simulation of the movements of beta particles in magnetic field using Geant4 program and observed experimentally using gafchromic film irradiated by beta emitter, based on the assumption that the volume of interaction of beta radiation is reduced thus causing more localized damage on the target tissue.

The beta particles tended to have circular movements in the magnetic field and their ranges were shortened when the magnitude of magnetic field was increased.

We found that beta particles tracing outward the point source in random directions were scattering in spherical geometry in the medium, and that the geometrical distribution becomes elliptical when magnetic field is applied because of the shortening of the ranges of beta particles perpendicular to the magnetic field. The shortening in the ranges of particles increases as the magnitude of

magnetic field is increased. Therefore, particles from the source accumulate more in the center when magnetic field is applied. This causes the radiation dose to condense in the center. Thus, as the applied magnetic field increases, the irradiated volume gets smaller, the particle hit number per unit length increases close to the center.

In conclusion, radiation may be focused and irradiation of the normal tissues can be prevented while increasing the target dose in the treatments with radioactive isotopes. Although it is not possible to use strong magnetic field in the clinical targeted therapy applications today, it may be possible in the future to shape the distribution of beta particles on the target tissue through magnetic field as desired.

Ethics

Ethics Committee Approval: The study was approved by the Dokuz Eylül University Local Ethics Committee (protocol number: 121/2009 and 122/2009).

Informed Consent: Not required.

Peer-review: Externally and internally peer-reviewed.

Authorship Contributions

Concept: H.D., K.A., Design: H.D., K.A., Data Collection or Processing: B.Ç., S.S., T.E., Analysis or Interpretation: B.Ç., S.S., H.D., K.A., H.E, Literature Search: B.Ç., S.S., Writing: B.Ç., K.A., H.D.

Conflict of Interest: No conflict of interest was declared by the authors.

Financial Disclosure: The authors declared that this study received no financial support.

References

1. Murray T, Hilditch TE. Therapeutic Applications of Radiopharmaceuticals. In: Sampson CB (ed). Texbook of Radiopharmacy Theory and Practise, Amsterdam, 3rd ed. Gordon and Brech Science Publishrs, 1999, 369.
2. Jevremovic T. Nuclear principles in engineering. Springer Science+Business Media, New York, 2005.
3. Alfassi ZB, Bonardi M, Groppi F, Menapace E. A new alpha-emitter for nuclear medicine: 230U. J Radioanal Nucl Chem 2006;2:483-487.
4. Raylman RR, Hammer BE, Christensen NL. Combined MRI-PET scanner: a Monte Carlo evaluation of the improvements in PET resolution due to the effects of a static homogeneous magnetic field. IEEE Trans Nucl Sci 1996;43:2406-2412.
5. Shih CC. High energy electron radiotherapy in a magnetic field. Med Phys 1975;2:9-13.
6. Raylman RR, Wahl RL. Magnetically enhanced radionudide therapy. J Nucl Med 1994;35:157-163.
7. Raylman RR, Wahl RL. Magnetically enhanced protection of bone marrow from beta particles emitted by bone-seeking radionuclides: theory of application. Med Phys 1995;22:1285-1292.
8. Agostinelli S, Allison J, Amako K, Apostolakis J, Araujo H, Arce P, Asai M, Axen D, Banerjee S, Barrand G, Behner F, Bellagamba L, Boudreau J, Broglia L, Brunengo A, Burkhardt H, Chauvie S, Chuma J, Chytracek R, Cooperman G, Cosmo G, Degtyarenko P, Dell'Acqua A, Depaola G, Dietrich D, Enami R, Feliciello A, Ferguson C, Fesefeldt H, Folger G, Foppiano F, Forti A, Garelli S, Giani S, Giannitrapani R, Gibin D, Gómez Cadenas JJ, González I, Gracia Abril G, Greeniaus G, Greiner W, Grichine V, Grossheim A, Guatelli S, Gumplinger P, Hamatsu R, Hashimoto K, Hasui H, Heikkinen A, Howard A, Ivanchenko V, Johnson A, Jones FW, Kallenbach J, Kanaya N, Kawabata M, Kawabata Y, Kawaguti M, Kelner S, Kent P, Kimura A, Kodama T, Kokoulin R, Kossov M, Kurashige H, Lamanna E, Lampén T, Lara V, Lefebure V, Lei F, Liendl M, Lockman W, Longo F, Magni S, Maire M, Medernach E, Minamimoto K, Mora de Freitas P, Morita Y, Murakami K, Nagamatu M, Nartallo R, Nieminen P, Nishimura T, Ohtsubo K, Okamura M, O'Neale S, Oohata Y, Paech K, Perl J, Pfeiffer A, Pia MG, Ranjard F, Rybin A, Sadilov S, Di Salvo E, Santin G, Sasaki T, Savvas N, Sawada Y, Scherer S, Sei S, Sirotenko V, Smith D, Starkov N, Stoecker H, Sulkimo J, Takahata M, Tanaka S, Tcherniaev E, Safai Tehrani E, Tropeano M, Truscott P, Uno H, Urban L, Urban P, Verderi M, Walkden A, Wander W, Weber H, Wellisch JP, Wenaus T, Williams DC, Wright D, Yamada T, Yoshida H, Zschiesche D. Geant4-a simulation toolkit. Nuclear Instruments and Methods in Physics Research 2003;506:250-303.
9. Kossert K, Schrader H. Activity standardization by liquid scintillation counting and half-life measurements of 90Y. Appl Radiat Isot 2004;60:741-749.
10. Dezarn WA, Cessna JT, DeWerd LA, Feng W, Gates VL, Halama J, Kennedy AS, Nag S, Sarfaraz M, Sehgal V, Selwyn R, Stabin MG, Thomadsen BR, Williams LE, Salem R; American Association of Physicists in Medicine. Recommendations of the American Association of Physicists in Medicine on dosimetry, imaging, and quality assurance procedures for 90Y microsphere brachytherapy in the treatment of hepatic malignancies. Med Phys 2011;38:4824-4845.
11. Sankar A, Ayyangar KM, Nehru RM, Kurup PG, Murali V, Enke CA, Velmurugan J. Comparison of Kodak EDR2 and Gafchromic EBT films for intensity-modulated radiation therapy dose distribution verification. Med Dosim 2006;31:273-282.
12. Butson MJ, Cheung T, Yu PK. Weak energy dependence of EBT Gafchromic film dose response in the 50 kVp-10MVp X-ray range. Appl Radiat Isot 2006;64:60-62.
13. Fuss M, Sturtewagen E, De Wagter C, Georg D. Dosimetric characterization of GafChromic EBT film and its implications on film dosimetry quality assurance. Phys Med Biol 2007;52:4211-4225.
14. Rault E, Vandenberghe S, Staelens S, Lemahieu I. Optimization of Yttrium-90 Bremsstrahlung Imaging with Monte Carlo Simulations. Springer, Verlag Berlin Heidelberg, 2009;22:500-504.
15. Gudkov SV, Shilyagina NY, Vodeneev VA, Zvyagin AV. Targeted Radionuclide Therapy of Human Tumors. Int J Mol Sci. 2015:17.
16. Goldenberg DM, Chang CH, Rossi EA, J W, McBride, Sharkey RM. Pretargeted molecular imaging and radioimmunotherapy. Theranostics 2012;2:523-540.
17. Maxon HR, Englaro EE, Thomas SR, Hertzberg VS, Hinnefeld JD, Chen LS, Smith H, Cummings D, Aden MD. Radioiodine-131 therapy for well-differentiated thyroid cancer–a quantitative radiation dosimetric approach: outcome and validation in 85 patients. J Nucl Med 1992;33:1132-1136.
18. Meredith R, Wessels B, Knox S. Risks to normal tissues from radionuclide therapy. Semin Nucl Med 2008;38:347-357.
19. Vallabhajosula S, Goldsmith SJ, Hamacher KA, Kostakoglu L, Konishi S, Milowski MI, Nanus DM, Bander NH. Prediction of myelotoxicity based on bone marrow radiation-absorbed dose: radioimmunotherapy studies using 90Y- and 177Lu-labeled J591 antibodies specific for prostate-specific membrane antigen. J Nucl Med 2005;46:850-858.
20. Enge H. Introduction to Nuclear Physics, 2nd ed. Reading, MA: Addison-Wesley, 1966.
21. Wirrwar A, Vosberg H, Herzog H, Halling H, Weber S, Muller-Gartner HW. 4.5 tesla magnetic field reduces range of high-energy positrons-potential implications for positron emission tomography. IEEE Trans Nucl Sc 1997;2:184-189.
22. Desbrée A, Pain F, Gurden H, Zimmer L, Pinot L, Lani`ece P, Mastrippolito R. Combining the radiosensitive beta microprobe to nuclear magnetic resonance: theoretical approach for in vivo studies in small animals. J Neurosci Methods 2004;140;47-52.

23. Christensen NL, Hammer BE, Heil BG, Fetterly K. Positron emission tomography within a magnetic field using photomultiplier tubes and lightguides. Phys Med Biol 1995;40:691-697.
24. Iida H, Kanno I, Miura S, Murakami M, Takahashi K, Uemura K. A simulation study of a method to reduce positron annihilation spread distributions using a strong magnetic field in positron emission tomography. IEEE Trans Nucl Sci 1986;33:597-600.
25. Rickey DW, Gordon R, Huda W. On lifting the inherent limitations of positron emission tomography by using magnetic fields (MagPET). Automedica 1991;14:355-369.
26. Kexin Y. Explanation of electromagnetic wave and induction by variation of electric fluxline and the deduction of magnetism rooted in constancy of light velocity. Applied Physics Research 2014;6:112-126.
27. Raaijmakers AJ, Raaymakers BW, Lagendijk JJ. Experimental verification of magnetic field dose effects for the MRI-accelerator. Phys Med Biol 2007;52:4283-4291.
28. Raylman RR, Clavo AC, Crawford SC, Recker B, Wahl RL. Magnetically-enhanced radionuclide therapy (MERiT): in vitro evaluation. Int J Radiat Oncol Biol Phys 1997;37:1201-1206.

Original Article
Mol Imaging Radionucl Ther 2017;26:62-68 DOI:10.4274/mirt.08760

Lu-177-PSMA-617 Prostate-Specific Membrane Antigen Inhibitor Therapy in Patients with Castration-Resistant Prostate Cancer: Stability, Bio-distribution and Dosimetry

Kastrasyona Dirençli Prostat Kanseri Hastalarında Lu-177-PSMA-617 ile Prostat Spesifik Membran Antijen İnhibitor Tedavisi: Kararlılık, Biyodağılım ve Dozimetri

Levent Kabasakal[1], Türkay Toklu[2], Nami Yeyin[1], Emre Demirci[3], Mohammad Abuqbeitah[1], Meltem Ocak[4], Aslan Aygün[1], Emre Karayel[1], Hüseyin Pehlivanoğlu[1], Nalan Alan Selçuk[2]

[1]*İstanbul University Cerrahpaşa Faculty of Medicine, Department of Nuclear Medicine, İstanbul, Turkey*
[2]*Yeditepe University Faculty of Medicine, Department of Nuclear Medicine, İstanbul, Turkey*
[3]*Şişli Etfal Training and Research Hospital, Clinic of Nuclear Medicine, İstanbul, Turkey*
[4]*İstanbul University Faculty of Pharmacy, Department of Pharmaceutical Technology, İstanbul, Turkey*

Abstract

Objective: The aim of the study was to estimate the radiation-absorbed doses and to study the *in vivo* and *in vitro* stability as well as pharmacokinetic characteristics of lutetium-177 (Lu-177) prostate-specific membrane antigen (PSMA)-617.

Methods: For this purpose, 7 patients who underwent Lu-177-PSMA therapy were included into the study. The injected Lu-177-PSMA-617 activity ranged from 3.6 to 7.4 GBq with a mean of 5.2±1.8 GBq. The stability of radiotracer in saline was calculated up to 48 h. The stability was also calculated in blood and urine samples. Post-therapeutic dosimetry was performed based on whole body and single photon emission computed tomography/computed tomography (SPECT/CT) scans on dual-headed SPECT/CT system.

Results: The radiochemical yield of Lu-177-PSMA-617 was >99%. It remained stable in saline up to 48 h. Analyses of the blood and urine samples showed a single radioactivity peak even at 24 hours after injection. Half-life of the distribution and elimination phases were calculated to be 0.16±0.09 and 10.8±2.5 hours, respectively. The mean excretion rate was 56.5±8.8% ranging from 41.5% to 65.4% at 24 h. Highest radiation estimated doses were calculated for parotid glands and kidneys (1.90±1.19 and 0.82±0.25 Gy/GBq respectively). Radiation dose given to the bone marrow was significantly lower than those of kidney and parotid glands ($p<0.05$) (0.030±0.008 Gy/GBq).

Conclusion: Lu-177-PSMA-617 is a highly stable compound both *in vitro* and *in vivo*. Lu-177-PSMA-617 therapy seems to be a safe method for the treatment of castration-resistant prostate cancer patients. The fractionation regime that enables the longest duration of tumor control and/or survival will have to be developed in further studies.

Keywords: PSMA, prostate-specific membrane antigen, Lu-177-PSMA, prostate cancer, castration-resistant prostate cancer, radionuclide therapy

Address for Correspondence: Levent Kabasakal MD, İstanbul University Cerrahpaşa Faculty of Medicine, Department of Nuclear Medicine, İstanbul, Turkey
Phone: +90 532 366 79 08 E-mail: kabasakal@tsnm.org **Received:** 26.06.2016 **Accepted:** 27.04.2017

Öz

Amaç: Çalışmanın amaçları lutesyum-177 (Lu-177) prostat-spesifik membran antijen (PSMA)-617 tedavisinde absorbe edilen dozları hesaplamak, radyofarmasötiğin *in vivo* ve *in vitro* kararlılığını araştırmak ve farmakokinetik özelliklerini değerlendirmektir.

Yöntem: Bu amaçla 7 hasta çalışmaya dahil edilmiştir. Hastalara 3,6 ila 7,4 GBq arasında değişen dozlarda ortalama 5,2±1,8 GBq Lu-177-PSMA-617 tedavi amacıyla verildi. Radyofarmasötiğin kararlılığı 48 saat süre ile serum fizyolojik içerisinde bekletilerek hesaplandı. Kararlılık ayrıca kan ve idrar örneklerinden de hesaplandı. Tedavi sonrası radyasyon dozu hesaplaması tüm vücut tek foton emisyon bilgisayarlı tomografi/bilgisayarlı tomografi görüntülerinden yapıldı.

Bulgular: Lu-177-PSMA-617'nin radyokimyasal verimliliği >%99 olarak bulundu. Serum fizyolojik içerisinde 48 saat bozulmadan kaldı. Kan ve idrar örneklerinde yapılan yüksek performanslı sıvı kromotografisi ölçümlerinde 24 saat sonra bile tek bir zirve verdi. Dağılım ve eliminasyon fazlarının yarılanma zamanları sırasıyla 0,16±0,09 ve 10,8±2,5 saat olarak hesaplandı. Ortalama 24 saat ekskresyon hızı %56,5±8,8 olarak bulundu ve ekskresyon hızı %41,5'den %65,4'e kadar değişim gösterdi. Hesaplanan en yüksek radyasyon dozu parotis bezleri ve böbrekler için bulundu ve sırasıyla 1,90±1,19 and 0,82±0,25 Gy/GBq idi. Kemik iliğine verilen radyasyon dozu böbrekler ve parotis beziyle karşılaştırıldığında istatistiksel olarak çok düşüktü ($p<0,05$) (0,030±0,008 Gy/GBq).

Sonuç: Lu-177-PSMA-617 *in vivo* ve *in vitro* şartlarda oldukça kararlı bir bileşik olarak gözükmektedir. Lu-177-PSMA-617 tedavisi kastrasyona dirençli prostat kanseri hastalarında kullanılabilecek oldukça güvenli bir radyofarmasötik olarak gözükmektedir. Hastalarda en uzun tümör kontrolü sağlayan fraksiyone tedavi yöntemi ileri çalışmalarla geliştirilmelidir.

Anahtar kelimeler: PSMA, prostat spesifik membran antijen, Lu-177-PSMA, prostat kanseri, kastrasyona dirençli prostat kanseri, radyonüklit tedavi

Introduction

Prostate-specific membrane antigen (PSMA) is a type 2 membrane glycoprotein that acts as a glutamate carboxypeptidase enzyme. It is highly expressed by all prostate cancers and its expression increases with increasing tumor aggressiveness (1,2,3). The unique expression of PSMA and ligand binding internalization of the PSMA via clathrin-coated pits and subsequent endocytosis makes it an excellent target for prostate cancer imaging and therapy using gallium-68 (Ga-68) and lutetium-177 (Lu-177) labeled ligands. Glu-NH-CO-NH-Lys-[Ga-68-(HBED-CC)] (Ga-68-PSMA-11) has been suggested as a novel tracer that can detect prostate cancer relapses and metastases with high contrast by targeting the PSMA (4,5,6,7,8). Also, therapeutic radiopharmaceutical Lu-177-PSMA-617 seems to be a promising novel tracer for systemic radionuclide therapy in patients with castration-resistant prostate cancer (9,10).

The basic principle of radionuclide therapy is to apply the maximum justifiable dose that does not cause serious toxicity in order to get an effective antitumor effect. The target organs for Lu-177-PSMA-617 therapy are the kidneys, parotid glands, and the bone marrow. In order to avoid toxicity, the amount of radiation dose given to target organs has to be estimated. Before introducing therapeutic applications we have performed a pre-therapy dosimetry study, and the initial results suggested that Lu-177-PSMA-617 therapy is a safe method (11). The target organs were the parotid glands rather than kidneys and bone marrow. The organ radiation doses were within acceptable ranges, however, there was a substantial individual variance that indicates that patient dosimetry is mandatory.

Therefore, we aimed to estimate the radiation-absorbed doses to dose limiting organs after systemic therapy with Lu-177-PSMA-617 in patients with castration-resistant prostate cancer. In addition, we also studied the *in vivo* and *in vitro* stability and pharmacokinetic characteristics of Lu-177-PSMA-617.

Materials and Methods

Patients

In order to calculate the radiation absorbed doses, 7 patients were included into the study. All patients had histopathological diagnosis of prostate cancer. The ages ranged from 66 to 82 years (mean 71±5.2 years). Patients had prostatic surgery (n=2) and radiation therapy (n=5). All patients had androgen deprivation therapy and chemotherapy. All patients had increasing blood PSA levels, despite chemotherapy. The Gleason score was 9 in 4 patients, 8 in 3 patients. Blood PSA levels ranged from 4.2 to 219.0 ng/mL (mean 80.6±88.4 ng/mL). In order to decide the eligibility for Lu-177-PSMA-617 treatment all patients had Ga-68-PSMA-11 positron emission tomography/computed tomography imaging, and all patients had radiopharmaceutical uptake at the lesion site. All patients received a treatment of Lu-177-PSMA-617 with slow infusion in closed infusion equipment when the patients were in fasting state. The injected Lu-177-PSMA-617 activity ranged from 3.6 to 7.4 GBq with a mean of 5.2±1.8 GBq. The amount of Lu-177-PSMA-617 activity was decided empirically according to the tumor load of the patient in bones. Patients with widespread metastases in bones received a lower amount of radiopharmaceutical. Dosimetry calculations could be made in 6 patients due to missing

data in one patient (Table 1). The study was approved by the Cerrahpaşa Medical Faculty Local Ethical Committee (protocol number: 830458809/604.01/02-268589).

Preparation of Lu-177-PSMA-617

The radiolabeling of PSMA-617 (10) was performed in a hotcell using Lu-177 Cl_3 (47 MBq/nmol of ligand) in 0.05 mol L^{-1} HCl (Perkin Elmer, USA) with sodium ascorbate buffer pH 4.5 (Polatom, Otwock-Swierk Poland) at 95 °C for 15 minutes. After cooling down of the reaction vial to room temperature the volume was adjusted to 2 mL with saline and 0.5-1.0 mL of sterile DTPA solution (3 mg mL^{-1} DTPA in saline) was added. After sterile filtration of this preparation to a sterile vial the volume was completed to 20 mL with sterile saline under aseptic conditions. Radiochemical purity was determined by instant thin layer chromatography (ITLC)-silica gel and radio-high performance liquid chromatography (HPLC) and was found as ≥98%.

Stability of Lu-177-PSMA-617

The prepared patient dose of Lu-177-PSMA-617 (3.7 GBq) was incubated in saline at 37 °C up to 48 h. At determined time points incubation solution sample was injected to the reversed-phase (RP)-HPLC for evaluating the *in vitro* stability of the patient dose up to 48 h. In 7 patients *in vivo* stability was checked by using blood samples obtained at 0-3, 30, 60, 120, 180 min and using urine samples obtained up to 24 h after injection of Lu-177-PSMA-617. Blood samples received from patients were precipitated with acetonitrile (1:1) and then vortexed. The precipitate was separated by centrifugation (5 min at 14680 rpm). For the RP-HPLC analysis, the supernatant was diluted with bi-distilled water (1:1), filtered and then injected into RP-HPLC. Collected urine samples from patients were diluted with bi-distilled water, filtered and immediately analyzed by RP-HPLC. Excreted urine of each patient was collected for 24 hours and 10 mL urine samples were measured in a dose calibrator and excretion rate of radiopharmaceutical was calculated.

Imaging and Dosimetry

Post-therapeutic dosimetry was performed based on whole body and single photon emission computed tomography/computed tomography (SPECT/CT) scans on dual-headed Symbia T16 SPECT/CT system (Siemens Medical Solutions, Erlangen, Germany) with 3/8-inch crystal thickness. Whole body scans (WBS) were performed using medium energy parallel hole collimators at time marks of 4, 24, 48 and 120 hours after administration of the prescribed treatment activity. Scan parameters include single energy peak at 208 keV with window width of 15%, 256×1024 matrix size with pixel size of 2.4×2.4 mm^2, 25 cm/min scan speed. Triple energy window-scatter correction (TEW-SC) was applied to all images using lower and upper scatter energy windows at 180 keV and 235 keV with window widths of 10%.

Two-bed SPECT/CT scan for each patient was performed only after 24th hour WBS to avoid unnecessary exposure to CT due to subsequent scans. Matrix size in SPECT imaging was 128×128 with pixel size of 4.8×4.8 mm^2. Counts were collected in a non-circular orbit during 25 seconds per view and total of 96 views (48 for each head) per bed position. To correct photon attenuation, CT scan with 5 mm slice thickness were acquired after SPECT scan using parameters of 130 kVp and 60 mAs per slice. SPECT images were reconstructed using iterative reconstruction algorithm with collimator-detector response compensation (OSEM Flash 3D, 4 iterations, 8 subsets). TEW-SC was also applied with the parameters stated above. Count-to-activity calibration of SPECT images was performed using NEMA IEC Body Phantom. The larger fillable sphere in the phantom was filled with the solution of Lu-177 with activity concentration of 185 kBq/mL. The same acquisition and reconstruction parameters that has been used for patient examinations were employed. A volume of interest (VOI) was drawn around the sphere in 3D with a threshold of 40% of maximum count. To obtain the calibration factor, total counts in the VOI were equalized to the total activity in the sphere.

Kidneys, liver, parotid gland and the rest of the body were selected as source organs. Region of interests were drawn

Table 1. Patient characteristics and calculated radiation absorbed doses (Gy/GBq of Lu-177-PSMA-617) per organs

Patient	Age	GS	Treatment Activity (GBq)	PSA (ng/mL)	Parotid gland	Kidney	Bone marrow	Liver	Whole Body Residence time (h)
1	70	8	7.4	19	1.73	0.94	0.016	0.10	23
2	73	9	7.3	184	0.70	0.88	0.034	0.14	36
3	68	8	3.7	15	2.84	0.83	0.024	0.19	26
4	69	9	3.6	28	3.81	0.96	0.032	0.32	38
5	72	9	3.6	219	1.18	0.32	0.037	0.06	44
6	66	9	5.6	96	1.16	1.00	0.034	0.18	40
Mean	69.7	8.7	5.2	93.5	1.90	0.82	0.030	0.17	34.5
SD	2.6	0.5	1.8	89.4	1.19	0.25	0.008	0.09	8.2

SD: Standard deviation, GS: Gleason score, h: Hour, PSA: Prostate-specific antigen

over the source regions on anterior and posterior WBS images for all time points. Total counts for each source organ were determined by conjugate view method with geometric background subtraction as described in MIRD Pamphlet No.16 (12). To perform geometric background subtraction, required body and mean organ thicknesses were determined from CT images of the SPECT/CT scan. Total activity in source organs at 24 hours after p.i. were determined from SPECT images by drawing VOIs around the source organ in 3D with the threshold of 40% of central mean counts of each organ. Counts in the VOIs were converted to activity by multiplication with the calibration factor described above. A conversion factor for each source organ was obtained from quotient of the organ counts of the 24th hour WBS to the activity in the organ determined from 24th hour SPECT imaging to convert WBS counts to activity for the other time points.

OLINDA/EXM (version 1.1) software was used to calculate the absorbed dose according to MIRD scheme. Both male and female adult phantoms were used. The source organ masses determined from CT slices as well as the total body mass were adjusted in the software. As the parotid glands are not included in the phantoms, unit density sphere model was used to estimate self-dose to the glands. Time integrated activity coefficients were determined using fit functions of the software.

Absorbed dose to the bone marrow was calculated from blood samples at different time points of 3, 10, 20, 40, 60 and 90 minutes, 2, 3, 24, 48 and 72 hours after the start of Lu-177-DKFZ-617 infusion, and the whole body activity was determined from the WBSs according to the EANM Guideline (13). The red marrow to blood ratio of 1 was selected for calculations.

Statistical Analysis

All results were expressed as mean±SD. For statistical analysis, a dedicated statistical software was used (StatPlus:mac v5. AnalystSoft Inc. BC. CA). Wilcoxon test was used to compare different groups. A p value lower than 0.05 was considered as significant.

Results

Stability and Bio-distribution

The radiochemical yield of Lu-177-PSMA-617 was >99% by RP-HPLC and 98.7±0.97% by ITLC. The radiopharmaceutical remained stable in saline up to 48 h after preparation, and radiochemical purity was found >98% at 48 h incubation time point (Figure 1). RP-HPLC analyses of the blood and urine samples showed a single radioactivity peak corresponding to Lu-177-PSMA-617 even at 24 hours after injection (Figure 2 and 3). There was no other peak corresponding to metabolized Lu-177 PSMA-617. Blood time activity curve showed a rapid bi-exponential clearance curve (Figure 4). Half-life of the distribution phase was calculated to be 0.16±0.09 hours and the half-life of elimination phase was calculated to be 10.8±2.5 hours. Total body residence time showed great variation among patients and it was ranged from 23.1 hours to 44.0 hours with a mean value of 37.5±7.5 hours. Almost half of the injected amount of radiopharmaceutical was excreted

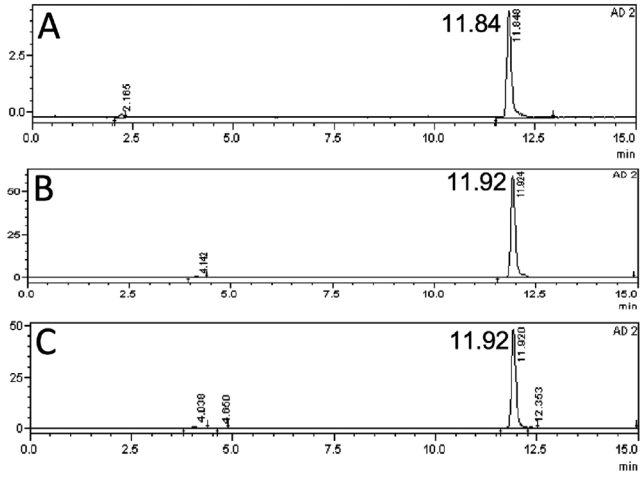

Figure 1. Reversed-phase-high performance liquid chromatography (RP-HPLC) profiles of Lu-177-PSMA-617 (the RP-HPLC elution time of radioligand is in between 11.7-11.96 min) in 100 mCi patient dose incubated in saline at 37 °C A) at 0-3 min, B) at 24 h, C) at 48 h

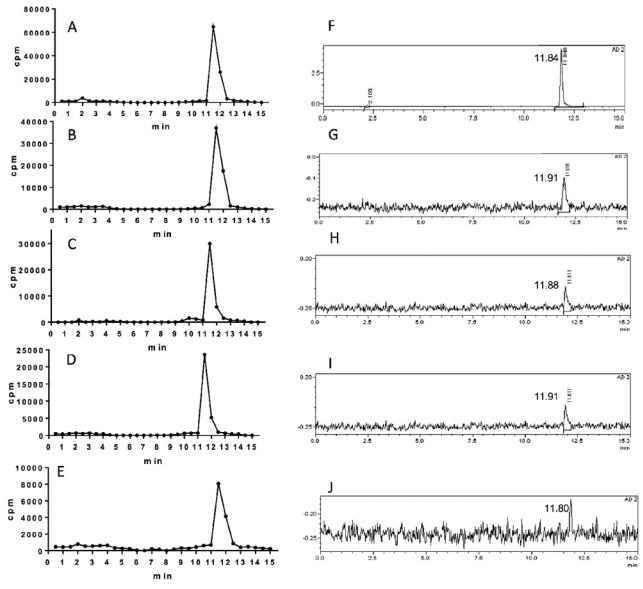

Figure 2. Reversed-phase-high performance liquid chromatography (RP-HPLC) profiles of Lu-177-PSMA-617 (the RP-HPLC elution time of radioligand is in between 11.7-11.96 min) in blood after 100 mCi injection of radioligand in a patient [A) 0-3 min, B) 30 min, C) 60 min, D) 120 min, E) 180 min] and 200 mCi injection of radioligand [F) 0-3 min, G) 30 min, H) 60 min, I) 120 min, J) 180 min]

within 24 hours. The mean excretion rate of injected radiopharmaceutical amount was 56.5±8.8%, ranging from 41.5% to 65.4%.

Toxicity

Patients were followed for 24 hours after infusion of radiopharmaceutical within 15 minutes. All patients tolerated the procedure very well and we did not observe any acute side effect. We did not observe any change in blood pressure, heart rate or body temperature. We did not observe any change in complete blood counts within one week.

Dosimetry

In whole body images obtained 4 hours p.i. there was high blood pool along with soft tissue uptake (Figure 5). Because of a rapid clearance from the blood, intense radiopharmaceutical uptake at the physiological uptake sites and at the sites of tumor lesions was observed in images obtained later. The radiopharmaceutical uptake decreased considerably in images obtained at 120 hours p.i.

The calculated radiation absorbed doses for each organ showed great variance among patients. The highest radiation estimated doses were calculated for the parotid glands and kidneys. For parotid glands the calculated mean radiation absorbed dose per GBq was 1.90±1.19 Gy. For the kidneys, the mean radiation absorbed dose was calculated to be 0.82±0.25 Gy/GBq. For the bone marrow, calculated radiation dose was significantly lower than those of kidney and parotid glands ($p<0.05$). The calculated radiation dose to the bone marrow was 0.030±0.008 Gy/GBq (Table 1).

The estimated maximum safe activities, at which organ doses do not exceed radiation absorbed dose constraints for parotid glands, kidneys and bone marrow, were calculated to be 21.7±12.8 GBq, 32.9±19.2 GBq and 73.8±27.1 GBq, respectively (Table 2).

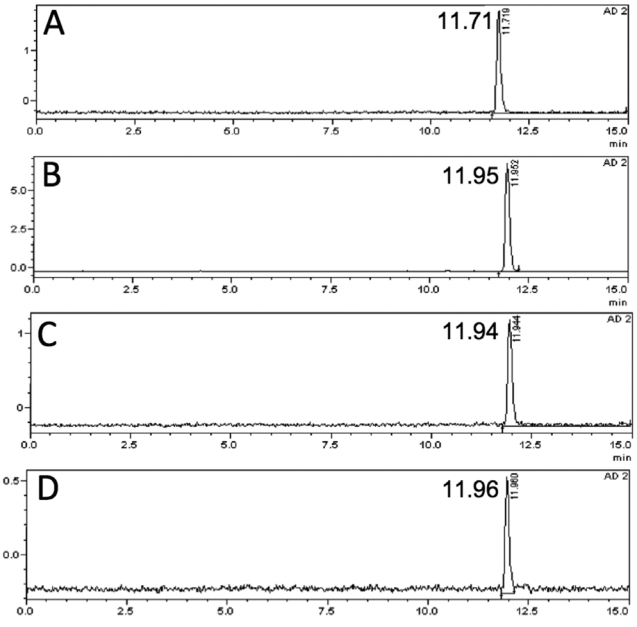

Figure 3. Reversed-phase-high performance liquid chromatography (RP-HPLC) profiles of Lu-177-PSMA-617 (the RP-HPLC elution time of radioligand is in between 11.7-11.96 min) in urine after 200 mCi injection of radioligand in a patient A) at 3 h, B) at 5 h, C) at 15 h, D) at 24 h

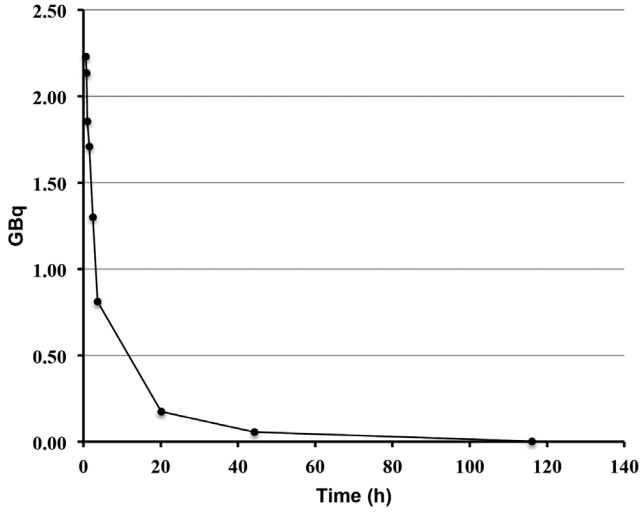

Figure 4. Mean blood-time radioactivity curve of all patients

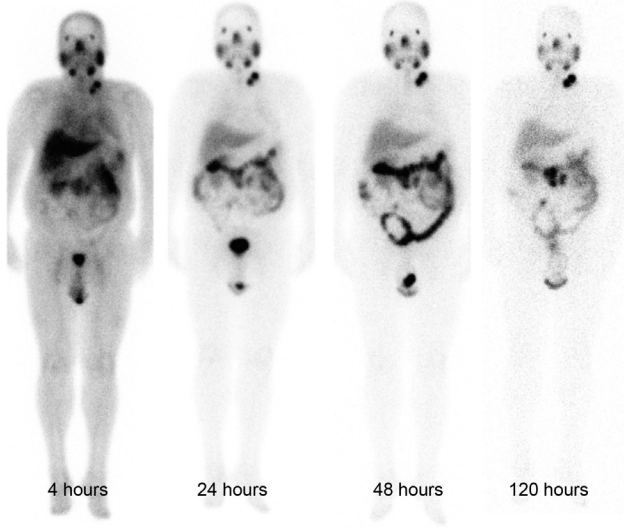

Figure 5. Lutetium-177 prostate-specific membrane antigen-617 whole body anterior images of a patient at different time points

Table 2. The calculated amount of radiopharmaceutical (GBq) to exceed radiation absorbed dose limits of organs at risk

Patient	Parotid gland (30 Gy)	Kidney (23 Gy)	Bone marrow (2 Gy)	Liver (32 Gy)
1	17.3	24.5	125.0	320.0
2	42.9	26.1	58.5	228.6
3	10.6	27.7	83.3	168.4
4	7.9	24.0	62.5	100.0
5	25.4	71.9	54.1	533.3
6	25.9	23.0	58.8	177.8
Mean	21.7	32.9	73.8	254.7
SD	12.8	19.2	27.1	154.8

SD: Standard deviation. Organ radiation absorbed dose constraints in parentheses

Discussion

The radiolabelling procedure of Lu-177-PSMA-617 is easy and it gives consistent high radiolabelling yields. Its radiochemical purity was over 98%. It remains stable in saline up to 48 h after radiolabelling, which provides time for quality control, transport of radiopharmaceutical from laboratory to the ward, and allows making a flexible therapy plan within the ward. It is also possible to make a slow infusion, if needed, for the administration of radiopharmaceutical to the patient. Administration to the patient was safe without any acute side effects and the patients tolerated it very well. After the administration, it is rapidly distributed within the body giving a bi-exponential blood clearance curve, which was consistent with the finding obtained in the pre-therapeutic dosimetry study published previously (11). Radiopharmaceutical also remained stable in blood and was excreted without any degradation. More than half of the administered radioactivity is excreted through the kidneys. During the first 24 hours, good hydration and frequent urination may protect the bladder from high radiation-absorbed dose. Due to its rapid excretion, it seems that Lu-177-PSMA-617 therapy can be given in an outpatient protocol according to national regulations, since 6 h after administration of the radiopharmaceutical the dose rate decreases to 20 μSv/h and the radiation exposure of caregivers remains below 5 mSv (14).

For the kidney, parotid gland and bone marrow, calculated radiation-absorbed doses were 0.82, 1.90 and 0.03 Gy/GBq respectively. These results are comparable with the pre-therapeutic dosimetry findings (11). The minor differences may be because of the different methodologies used between two studies, because 3D methods are not affected from the overlapping structures. Our results seem to be higher than the results of Delker et al. (15). They calculated the radiation-absorbed doses for kidney, salivary glands, and bone marrow as 0.6, 1.41 and 0.012 Gy/GBq, respectively. This difference can be attributed to the different time periods used for the calculation of absorbed doses. Delker et al. (15) have used a shorter time period for obtaining data and estimating residence time, which was only 72 h after injection as compared to our data, which was containing the data of 110 h after administration of radiopharmaceutical.

In accordance with the previous bio-distribution and dosimetry studies, the highest radiation absorbed dose was observed in salivary glands due to high uptake of the radiopharmaceutical and it seems to be the critical organ at risk rather than the kidney and bone marrow (11,12,13,14,15). Xerostomia is a frequent side effect of radiation therapy after exceeding 40 Gy of radiation doses, which decreases patient's quality of life (16,17). On the other hand, although salivary gland dysfunction is a common finding in patients treated with radioiodine, it is usually transient and persistent dysfunction rate is reported to be only 5% (18). As stated by Delker et al. (15), we also did not observe xerostomia in patients treated with Lu-177-PSMA-617 during follow-up.

Bone marrow absorbed dose is the major factor that limits radiopharmaceutical dose given to the patient and may have fatal consequences. The radiation absorbed dose given to the bone marrow is 0.030±0.008 Gy/GBq. In order not to exceed the 2 Gy limit to develop bone marrow toxicity, it seems that it is safe to administer up to 73.8 GBq (19). We agree with Delker et al. (15) that bone marrow toxicity seems to be unlikely with the suggested amounts of Lu-177-PSMA-617 for each cycle. However, bone marrow dose estimation in patients with prostate cancer which have extensive bone metastases using blood based dosimetry models may underestimate the absolute dose due to the existence of high radiopharmaceutical avid lesions which increase the dose delivered to bone marrow. Moreover, end-stage prostate cancer patients are extensively treated with chemotherapy and radiotherapy, which may potentially increase the risk of development of hematotoxicity even with a lower amount of radiation dose to the bone marrow.

The kidneys are important target organs due to their high radiotracer uptake and excretion. Based on the earlier experience obtained from conventional external

beam radiotherapy, the maximum kidney dose is generally accepted as 23 Gy (19). In order to reach this dose limit to the kidneys a mean of 32.9 GBq of Lu-177-PSMA-617 can be given. It seems that it is safe to administer usual doses without developing kidney toxicity.

Conclusion

In conclusion, radiolabelling of Lu-177-PSMA-617 is easy, and it is a highly stable compound both *in vitro* and *in vivo*. Lu-177-PSMA-617 therapy seems to be a safe method for the therapy of castration-resistant prostate cancer patients. The fractionation regime that enables the longest duration of tumor control and/or survival will have to be developed in further studies. It shows substantial difference among patients. Therefore, a patient specific dosimetric approach should be applied before therapy to prevent organ toxicity.

Ethics

Ethics Committee Approval: The study were approved by the Cerrahpaşa Medical Faculty Local Ethics Committee (Protocol number: 830458809/604.01/02-268589, **Informed Consent:** Obtained from all patients).

Peer-review: Externally and internally peer-reviewed.

Authorship Contributions

Surgical and Medical Practices: L.K., E.D., N.A.S., Concept: L.K., N.A.S., T.T., M.O., Design: T.T., N.Y., M.A., M.O., Data Collection or Processing: N.Y., A.A., H.P., E.K., M.O., Analysis or Interpretation: E.D., T.T., N.A.S., L.K., Literature Search: L.K., E.D., N.A.S., Writing: L.K., M.O., N.A.S., T.T., E.D.

Conflict of interest: The authors declare that they have no conflict of interest.

Financial Disclosure: The authors declared that this study received no financial support.

References

1. Wright GL Jr, Haley C, Beckett ML, Schellhammer PF. Expression of prostate-specific membrane antigen in normal, benign, and malignant prostate tissues. Urol Oncol 1995;1:18-28.
2. Perner S, Hofer MD, Kim R, Shah RB, Li H, Möller P, Hautmann RE, Gschwend JE, Kuefer R, Rubin MA. Prostate-specific membrane antigen expression as a predictor of prostate cancer progression. Hum Pathol 2007;38:696-701.
3. Silver DA, Pellicer I, Fair WR, Heston WD, Cordon-Cardo C. Prostate-specific membrane antigen expression in normal and malignant human tissues. Clin Cancer Res 1997;3:81-85.
4. Eder M, Schäfer M, Bauder-Wüst U, Hull WE, Wängler C, Mier W, Haberkorn U, Eisenhut M. 68Ga-complex lipophilicity and the targeting property of a urea-based PSMA inhibitor for PET imaging. Bioconjug Chem 2012;23:688-697.
5. Eder M, Schäfer M, Bauder-Wüst U, Haberkorn U, Eisenhut M, Kopka K. Preclinical evaluation of a bispecific low-molecular heterodimer targeting both PSMA and GRPR for improved PET imaging and therapy of prostate cancer. Prostate. 2014;74:659-668.
6. Afshar-Oromieh A, Malcher A, Eder M, Eisenhut M, Linhart HG, Hadaschik BA, Holland-Letz T, Giesel FL, Kratochwil C, Haufe S, Haberkorn U, Zechmann CM. PET imaging with a [68Ga] gallium-labelled PSMA ligand for the diagnosis of prostate cancer: biodistribution in humans and first evaluation of tumour lesions. Eur J Nucl Med Mol Imaging 2013;40:486-495.
7. Afshar-Oromieh A, Avtzi E, Giesel FL, Holland-Letz T, Linhart HG, Eder M, Eisenhut M, Boxler S, Hadaschik BA, Kratochwil C, Weichert W, Kopka K, Debus J, Haberkorn U. The diagnostic value of PET/CT imaging with the (68)Ga-labelled PSMA ligand HBED-CC in the diagnosis of recurrent prostate cancer. Eur J Nucl Med Mol Imaging 2015;42:197-209.
8. Kabasakal L, Demirci E, Ocak M, Akyel R, Nematyazar J, Aygun A, Halac M, Talat Z, Araman A. Evaluation of PSMA PET/CT imaging using a 68Ga-HBED-CC ligand in patients with prostate cancer and the value of early pelvic imaging. Nucl Med Commun 2015;36:582-587.
9. Kratochwil C, Giesel FL, Eder M, Afshar-Oromieh A, Benešová M, Mier W, Kopka K, Haberkorn U. [177Lu]Lutetium-labelled PSMA ligand-induced remission in a patient with metastatic prostate cancer. 2015;42:987-988.
10. Benešová M, Schäfer M, Bauder-Wüst U, Afshar-Oromieh A, Kratochwil C, Mier W, Haberkorn U, Kopka K, Eder M. Preclinical Evaluation of a Tailor-Made DOTA-Conjugated PSMA Inhibitor with Optimized Linker Moiety for Imaging and Endoradiotherapy of Prostate Cancer. J Nucl Med 2015;56:914-920.
11. Kabasakal L, AbuQbeitah M, Aygün A, Yeyin N, Ocak M, Demirci E, Toklu T. Pre-therapeutic dosimetry of normal organs and tissues of (177)Lu-PSMA-617 prostate-specific membrane antigen (PSMA) inhibitor in patients with castration-resistant prostate cancer. Eur J Nucl Med Mol Imaging 2015;42:1976-1983.
12. Siegel JA, Thomas SR, Stubbs JB, Stabin MG, Hays MT, Koral KF, Robertson JS, Howell RW, Wessels BW, Fisher DR, Weber DA, Brill AB. MIRD pamphlet no. 16: Techniques for quantitative radiopharmaceutical biodistribution data acquisition and analysis for use in human radiation dose estimates. J Nucl Med 1999;40:37S-61S.
13. Hindorf C, Glatting G, Chiesa C, Lindén O, Flux G; EANM Dosimetry Committee. EANM Dosimetry Committee guidelines for bone marrow and whole-body dosimetry. Eur J Nucl Med Mol Imaging 2010;37:1238-1250.
14. Demir M, Abuqbeitah M, Uslu-Beşli L, Yıldırım Ö, Yeyin N, Çavdar İ, Vatankulu B, Gündüz H, Kabasakal L. Evaluation of radiation safety in (177)Lu-PSMA therapy and development of outpatient treatment protocol. J Radiol Prot 2016;36:269-278.
15. Delker A, Fendler WP, Kratochwil C, Brunegraf A, Gosewisch A, Gildehaus FJ, Tritschler S, Stief CG, Kopka K, Haberkorn U, Bartenstein P, Böning G. Dosimetry for (177)Lu-DKFZ-PSMA-617: a new radiopharmaceutical for the treatment of metastatic prostate cancer. Eur J Nucl Med Mol Imaging 2016;43:42-51.
16. Deasy JO, Moiseenko V, Marks L, Chao KS, Nam J, Eisbruch A. Radiotherapy dose-volume effects on salivary gland function. Int J Radiat Oncol Biol Phys 2010;76 (Suppl 3):s58-63.
17. Grundmann O, Mitchell GC, Limesand KH. Sensitivity of salivary glands to radiation: from animal models to therapies. J Dent Res 2009;88:894-903.
18. Jeong SY, Kim HW, Lee SW, Ahn BC, Lee J. Salivary gland function 5 years after radioactive iodine ablation in patients with differentiated thyroid cancer: direct comparison of pre- and postablation scintigraphies and their relation to xerostomia symptoms. Thyroid 2013;23:609-616.
19. Sandström M, Garske-Román U, Granberg D, Johansson S, Widström C, Eriksson B, Sundin A, Lundqvist H, Lubberink M. Individualized dosimetry of kidney and bone marrow in patients undergoing 177Lu-DOTA-octreotate treatment. J Nucl Med 2013;54:33-41.

Original Article
Mol Imaging Radionucl Ther 2017;26:69-75 DOI:10.4274/mirt.54376

Efficacy of ^{18}F-2-fluoro-2-deoxy-D-glucose Positron Emission Tomography/Computerized Tomography for Bone Marrow Infiltration Assessment in the Initial Staging of Lymphoma

^{18}F-2-fluoro-2-deoksi-D-glukoz Pozitron Emisyon Tomografisi/Bilgisayarlı Tomografinin Lenfomanın İnisiyal Evrelemesinde Kemik İliği Tutulumunun Belirlenmesindeki Rolü

Ali Ozan Öner[1], Evrim Sürer Budak[2], Funda Aydın[3], Ozan Salim[4], Orhan Kemal Yücel[4], Bahar Akkaya[5], Tayfur Toptaş[6], Adil Boz[3], Akın Yıldız[3], Fırat Güngör[3], Levent Undar[4]

[1]*Afyon Kocatepe University Faculty of Medicine, Department of Nuclear Medicine, Afyonkarahisar, Turkey*
[2]*Antalya Training and Research Hospital, Clinic of Nuclear Medicine, Antalya, Turkey*
[3]*Akdeniz University Faculty of Medicine, Department of Nuclear Medicine, Antalya, Turkey*
[4]*Akdeniz University Faculty of Medicine, Department of Hematology, Antalya, Turkey*
[5]*Akdeniz University Faculty of Medicine, Department of Pathology, Antalya, Turkey*
[6]*Marmara University Faculty of Medicine, Department of Hematology, İstanbul, Turkey*

Abstract

Objective: Currently ^{18}F-2-fluoro-2-deoxy-D-glucose (^{18}F-FDG) positron emission tomography/computerized tomography (PET/CT) is being successfully used for staging and follow-up of Hodgkin's lymphoma (HL) and non-Hodgkin's lymphoma (NHL). Various studies have demonstrated that PET/CT effectively detects bone marrow involvement (BMI) and is concordant with bone marrow biopsy (BMB) findings, thus it is deemed as a complementary method. This study was aimed to evaluate ^{18}F-FDG-PET/CT efficiency for detection of BMI in HL and NHL.

Methods: The study included 172 lymphoma cases who were admitted to Akdeniz University Medical School Department of Nuclear Medicine for initial staging with PET/CT. Visual and semiquantitative assessments were performed for PET/CT scan findings of the cases. The maximum standard uptake (SUV_{max}) value was the quantitative parameter used for ^{18}F-FDG-PET scan. In visual assessment, bone marrow metabolic activity that is greater than the liver was considered as pathologic. For semiquantitative assessment, regions of interest were drawn for SUV_{max} estimation, which included iliac crest in cases with diffusely increased metabolic activity and the highest activity area in cases with focal involvement. BMB was considered as the reference test.

Results: On visual assessment of all the cases, PET/CT was found to yield 31% sensitivity and 85% specificity rate for detection of BMI. On visual assessment of HL cases, sensitivity rate was determined as 80%, and specificity as 78%, while in NHL cases the corresponding values were 24% and 90%, respectively. On semiquantitative assessment of HL cases, considering $SUV_{max} \geq 4$, sensitivity was found as 80% and specificity as 68%. In NHL patients, considering $SUV_{max} \geq 3.2$, sensitivity rate was detected as 65% and specificity as 58%.

Conclusion: In this study, a moderately high concordance was observed between PET/CT and BMB findings. PET/CT appears to be a significant method for detecting BMI. Although PET/CT is not a substitute for BMB, we suggest it can be used as a guide to biopsy site and a complementary imaging technique for BMB.

Keywords: Hodgkin's lymphoma, non-Hodgkin's lymphoma, positron emission tomography/computerized tomography, bone marrow biopsy

Address for Correspondence: Funda Aydın MD, Akdeniz University Faculty of Medicine, Department of Nuclear Medicine, Antalya, Turkey
Phone: +90 242 249 60 00 E-mail: afunda12@gmail.com **Received:** 28.09.2016 **Accepted:** 18.02.2017

Öz

Amaç: Günümüzde ^{18}F-2-fluoro-2-deoksi-D-glukoz (^{18}F-FDG) pozitron emisyon tomografisi/bilgisayarlı tomografi (PET/BT), Hodgkin lenfoma (HL) ve non-Hodgkin lenfomaların (NHL) evrelemesinde ve takibinde başarılı bir şekilde kullanılmaktadır. Değişik çalışmalarda PET/BT'nin kemik iliği tutulumunu göstermede etkinliği ve kemik iliği biyopsisi (KİB) ile uyumu gösterilmiş ve tamamlayıcı yöntem olarak kullanılması önerilmiştir. Biz de bu çalışmada HL ve NHL'de kemik iliği infiltrasyonunu değerlendirmede PET/BT'nin etkinliğini değerlendirmeyi amaçladık.

Yöntem: Çalışmaya Akdeniz Üniversitesi Tıp Fakültesi Nükleer Tıp Anabilim Dalı'nda başlangıç evreleme için PET/BT tetkiki yapılan 172 lenfoma olgusu dahil edilmiştir. Olguların PET/BT tetkikinde görsel ve semikantitatif değerlendirme yapıldı.^{18}F-FDG-PET tetkikinde kantitatif parametre olarak maksimum standart uptake değeri (SUV_{maks}) kullanıldı. Görsel değerlendirmede karaciğerden daha yüksek metabolik aktivite gösteren kemik iliği aktivitesi patolojik olarak değerlendirildi. Semikantitatif değerlendirmede ise kemik iliğinde diffüz metabolik aktivite artışı gösteren olgularda iliak kanattan, fokal tutulumda ise en yüksek aktivite gösteren alandan ilgi alanı çizdirilerek SUV_{maks} değeri hesaplandı. KİB sonuçları referans olarak alınmıştır.

Bulgular: Tüm olgular için görsel değerlendirmede PET/BT'nin kemik iliği infiltrasyonunu göstermede duyarlılığı %31, özgüllüğü %85 olarak saptanmıştır. HL olgularında görsel değerlendirmede duyarlılık %80, özgüllük %78; NHL olgularında ise duyarlılık %24, özgüllük %90 olarak bulunmuştur. Semikantitatif değerlendirmede HL'de SUV_{maks}≥4 alındığında duyarlılık %80, özgüllük %68 olarak saptanmıştır. NHL'de ise SUV_{maks}≥3,2 olarak belirlendiğinde duyarlılık %65, özgüllük %58 olarak bulunmuştur.

Sonuç: Bu çalışmada, çok yüksek olmamakla birlikte, PET/BT bulguları ile KİB sonuçları arasında uyum izlendi. PET/BT görüntülemenin kemik iliği infiltrasyonu olup olmadığını göstermede etkili bir yöntem olduğunu görmekteyiz. PET/BT'nin, KİB'nin yerini almamakla birlikte, biyopsi yapılabilecek bölgeyi göstermede yönlendirici ve KİB'yi tamamlayıcı bir görüntüleme yöntemi olarak kullanılabileceğini düşünmekteyiz.

Anahtar kelimeler: Hodgkin lenfoma, non-Hodgkin lenfoma, pozitron emisyon tomografisi/bilgisayarlı tomografi, kemik iliği biyopsisi

Introduction

Accurate staging of lymphomas is essential both to implement effective treatment protocols and minimize side effects (1). Identification of bone marrow infiltration (BMI) has an important role in staging (2). Bone marrow involvement indicates generalized disease in lymphoma patients, and the standard method established for its evaluation is bone marrow biopsy (BMB). BMB from unilateral iliac crest is the routine first-line method used for staging (3,4). However, this method has certain limitations since it is an invasive method and allows for evaluation of a limited part of the bone marrow. BMI can also be detected by imaging techniques. Computerized tomography (CT) detects cortical bone lesions and late stage bone changes. However, it has a low sensitivity rate for detecting early stage changes (5). Magnetic resonance (MR) is not used in routine practice since it is a sensitive but costly technique, which needs longer imaging time and is anatomically limited.

Currently, ^{18}F-2-fluoro-2-deoxy-D-glucose (^{18}F-FDG) positron emission tomography (PET/CT) is being successfully used for both staging and follow-up of Hodgkin's lymphoma (HL) and non-Hodgkin's lymphoma (NHL) (2,6,7). Various studies have demonstrated that PET/CT effectively detects bone marrow involvement and is concordant with BMB findings (1,5,8). Thus, it is deemed as a complementary method (9). This study aimed to evaluate the efficacy of ^{18}F-FDG-PET/CT in detection of BM infiltration in HL and NHL.

Materials and Methods

Patients

This study, approved by the Akdeniz University Medical School Local Ethics Committee, included histopathologically confirmed, treatment naïve 172 lymphoma cases (50 F, 122 M; age interval 3-85; mean age 45.37±21.14; 64 HL, 108 NHL) who underwent initial staging with PET/CT at Akdeniz University Medical School Department of Nuclear Medicine between July 2009 and December 2013. Patients included in the study did not have other concomitant malignancies. Additionally, patients did not receive any bone marrow stimulation therapy before PET/CT scanning. The maximum interval between PET/CT scan and BMB was 10 days.

Positron Emission Tomography/Computerized Tomography Scanning

Intravenous 0.1 mCi/kg ^{18}F-FDG was administered to each patient following 6 hours of fasting, with a blood glucose level below 200 mg/dL. The intravenous/oral contrast agent was administered. After 45-60 minutes of waiting period, PET/CT images were acquired from the vertex to the upper thigh with Siemens Biograph True Point PET/CT scanner (CT section thickness 3 mm, 110 mAs, 120 kV; 3 minutes per-bed PET) (Siemens, Erlangen, Germany) at the PET/CT unit. Attenuation corrected PET, CT and fusion PET/CT images were reviewed simultaneously; visual and semiquantitative assessments were performed. The maximum standard uptake value (SUV_{max}) was the

quantitative parameter used for ^{18}F-FDG-PET scan. In visual assessment, bone marrow metabolic activity that is greater than the liver was considered to be pathologic. For semiquantitative assessment, regions of interest (ROI) were drawn for SUV_{max} estimation, which included iliac crest in cases with diffusely increased metabolic activity and the highest activity area in cases with focal involvement.

Bone Marrow Biopsy

Unilateral BMB of the posterior iliac crest was performed by different hematologists as part of routine clinical evaluation, and the presence of marrow infiltration was interpreted by an experienced hematopathologist who was blinded to the PET/CT results. Trephine biopsy samples were analyzed following the standard procedures. BMB was considered as positive in the presence of lymphoma involvement. Although flow cytometric immunophenotyping of marrow aspirates can be performed, this method was not used for the diagnosis of bone marrow involvement.

Data Analysis

BM biopsy results were regarded as the reference test for evaluating BMI.

Cases with concordant findings in both PET/CT and BMB (both positive or negative) were evaluated as true positive or true negative results. Non-concordance between these two parameters was described as false negativity or false positivity.

The sensitivity and specificity rates, positive predictive value (PPV) and negative predictive value (NPV) of PET/CT for detecting BM infiltration were determined for all cases. Additionally, receiver operating characteristics (ROC) curves were formed to determine cut-off values for SUV_{max}. Analyzes were performed with PASW 18 (SPSS/IBM, Chicago, IL, USA) software.

Results

Among the 172 cases, BMI was detected by PET/CT in 33 (19.1%) and by BMB in 42 (24.4%) patients (Table 1). Among the 33 cases with infiltration on PET/CT, 11 had diffuse heterogeneous patchy accumulations while 22 had unifocal/multifocal accumulations. Within the 64 HL patients, BMI was detected by PET/CT in 17 (26.5%) and by BMB in 5 (7.8%) (Table 2), while among the 108 NHL patients, BMI was detected by PET/CT in 16 (14.8%) and by BMB in 37 (34.2%) (Table 3).

Concordance between PET/CT and BMB was observed in 123 (71%) of 172 patients. Both tests were negative in 110 patients and both were reported positive in 13 patients. A concordance between PET/CT and BMB was detected in 50 (78%) HL patients, both tests were negative in 46 and positive in 4 patients. Non-concordance was observed in 14 (22%) of these patients, 13 patients were positive on PET/CT but negative on BMB while 1 patient was positive on BMB but negative on PET/CT. Concordance was detected in 73 (67%) NHL patients, both tests were negative in 64 and positive in 9 patients. The tests were non-concordant in 35 patients, 7 patients were positive on PET/CT but negative on BMB while 28 patients were positive on BMB but negative on PET/CT.

On visual assessment of all the cases, PET/CT was found to have a 31% sensitivity and 85% specificity rate for detection of BMI with 39% PPV and 79% NPV (Table 4). Visual assessment of HL cases showed 80% sensitivity, 78% specificity with 24% PPV and 98% NPV (Table 4), while in NHL cases the corresponding values were 24%, 90%, 56% and 70%, respectively (Table 4).

Table 1. Distribution of the patients according to positron emission tomography/computerized tomography and bone marrow biopsy test results

Key			
frequency row percentage column percentage			
	BM		
PET	Negative	Positive	Total
Negative	110 79.14 84.62	29 20.86 69.05	139 100.00 80.81
Positive	20 60.61 15.38	13 39.39 30.95	33 100.00 19.19
Total	130 75.58 100.00	42 24.42 100.00	172 100.00 100.00

PET: Positron emission tomography/computerized tomography, BM: Bone marrow

Table 2. Distribution of the Hodgkin's lymphoma patients according to positron emission tomography/computerized tomography and bone marrow biopsy test results

Key			
frequency row percentage column percentage			
	BM		
PET	Negative	Positive	Total
Negative	46 97.87 77.97	1 2.13 20.00	47 100.00 73.44
Positive	13 76.47 22.03	4 23.53 80.00	17 100.00 26.56
Total	59 92.19 100.00	5 7.81 100.00	64 100.00 100.00

PET: Positron emission tomography/computerized tomography, BM: Bone marrow

Semiquantitative assessment was performed using SUV_{max} values and ROC curves based on BMB findings. Area under the ROC curve (AUC) estimated for all patients was 0.6386, that of HL patients was 0.7763 and NHL patients was 0.6534. Cut-off, sensitivity and specificity values were estimated using ROC curves for all patients and HL and NHL patient subgroups. The results were as follows, respectively; cut-off 3.5, 4, 3.2; sensitivity 59%, 80%, 65%; specificity 62%, 68%, 58% (Table 5).

Estimated mean SUV_{max} value was 12.02 g/mL for the 33 patients with positive findings on PET/CT; 11.67 g/mL for 13 patients who were positive on both PET/CT and BMB; and 12.25 g/mL for 20 patients who were positive on PET/CT but negative on BMB (Table 6).

Table 3. Distribution of the non-Hodgkin's lymphoma patients according to positron emission tomography/computerized tomography and bone marrow biopsy test results

Key			
frequency row percentage column percentage			
	BM		
PET	Negative	Positive	Total
Negative	64 69.57 90.14	28 30.43 75.68	92 100.00 85.19
Positive	7 43.75 9.86	9 56.25 24.32	16 100.00 14.81
Total	71 65.74 100.00	37 34.26 100.00	108 100.00 100.00

PET: Positron emission tomography/computerized tomography, BM: Bone marrow

Discussion

Initial evaluation including determination of anatomic distribution of the disease extent is an essential factor to predict both disease-free and overall survival in lymphoma patients. BM involvement in lymphoma indicates generalized disease and is a predictor of poor prognosis. Besides the role of BMI in primary staging, it has a specific clinical significance for guiding the treatment approach (2). In routine clinical practice, BMB is used to evaluate BM involvement. Although BMB is primarily a safe and risk-free procedure, complications such as bleeding or infection can rarely occur. Additionally, being an invasive and painful procedure can be a disadvantage for patients. In case of insufficient sampling, repeated biopsies may be required. There is no consensus on whether BMB should be performed uni- or bi-laterally, thus biopsies are usually

Table 4. Sensitivity, specificity, positive predictive value and negative predictive value (95% confidence interval) of positron emission tomography/computerized tomography with respect to bone marrow biopsy in the whole population and Hodgkin's lymphoma and non-Hodgkin's lymphoma subgroups

	n	Sensitivity	Specificity	Positive predictive value	Negative predictive value
All patients	172	30.95%	84.62%	39.39%	79.14%
Hodgkin lymphoma	64	80%	77.97%	23.53%	97.87%
Non-Hodgkin lymphoma	108	24.32%	90.14%	56.25%	69.57%

Table 5. Receiver operating characteristics estimated area under curve with 95% confidence intervals, cut off, sensitivity and specificity values for the whole population and for Hodgkin's lymphoma and non-Hodgkin's lymphoma subgroups

	All patients	HL	NHL
AUC	0.6386	0.7763	0.6534
Cut off	3.5	4	3.2
Sensitivity	59%	80%	65%
Specificity	62%	68%	58%

AUC: Area under curve, HL: Hodgkin's lymphoma, NHL: Non-Hodgkin's lymphoma

Table 6. Numeric distribution and mean maximum standard uptake values for patients with positive results on positron emission tomography/computerized tomography

	PET/CT (+)	PET/CT (+)/BMB (+)	PET/CT (+)/ BMB (-)
n	33	13	20
Mean SUV_{max} (g/mL)	12.02	11.67	12.25

PET/CT: Positron emission tomography/computerized tomography, SUV_{max}: Maximum standard uptake value, BMB: Bone marrow biopsy

obtained from unilateral iliac crest blindly, which may lead to high false negative rates. In light of the mentioned reasons, there is growing interest in the search for accurate non-invasive methods to evaluate BMI. ^{18}F-FDG-PET/CT is a hybrid imaging technique used for primary staging, evaluating treatment response, re-staging and for follow-up after complete remission in lymphoma patients. Although, due to the limited number of studies, its role in evaluating bone/BM involvement is not well established, available results in the literature are promising (5,8).

Studies in the literature include mixed populations involving both HL and NHL patients. Cortés-Romera et al. (10) evaluated ^{18}F-FDG-PET/CT performance for detecting BMI with reference to BMB in their study on 147 patients, comprising of 84 diffuse large B-cell lymphoma (DLBCL) and 63 HL patients. This study showed concordance between the two tests in 128 patients (87%) (74 DLBCL, 54 HL). Among these, both tests were reported positive in 21 and negative in 107 patients. Non-concordance was observed in 19 (14%) patients, 18 of which had negative BMB results although involvement was detected on ^{18}F-FDG-PET/CT, indicating BMB was not obtained from active involvement sites. As a result of this study, ^{18}F-FDG-PET/CT was reported to be 95% sensitive, 86% specific with 87% accuracy, 54% PPV and 99% NPV for detecting BMI. It was concluded that ^{18}F-FDG-PET/CT had higher BMI detection rates in DLBCL and HL patients and in serving as a guide to biopsy sites, and that it can be used as a supplement to BMB (10).

In our study, among the 172 patients, 64 were diagnosed as HL and 108 as NHL. Thirty-three (19.1%) patients were found positive by ^{18}F-FDG-PET/CT and 42 (24.4%) were positive on BMB. Concordance between the two tests was observed in 123 of the 172 patients (71%). Both tests were reported negative in 110 patients and both were positive in 13. Based on the total study population in the current study, ^{18}F-FDG-PET/CT was detected to have 31% sensitivity and 85% specificity rate in detecting BMI with 39% PPV and 79% NPV. Additionally, AUC and cut-off values for the whole study population were 0.6386 and 3.5, respectively.

Similar studies on separate groups of HL and NHL patients are also available in the literature. In the study by Muzahir et al. (11), BMB from bilateral iliac crests were obtained from 122 HL patients and ^{18}F-FDG-PET/CT findings were compared to these results that are considered as the gold standard. Accordingly, ^{18}F-FDG-PET/CT was found to be 100% sensitive, 76.57% specific for detecting BMI in HL patients, with 78.62% diagnostic accuracy, 76.57% NPV and 29.72% PPV. The high sensitivity of ^{18}F-FDG-PET/CT in this study was attributed to the positive ^{18}F-FDG-PET/CT results in all of the BMB positive patients (11).

In the meta-analysis by Cheng and Alavi (12) including 7 studies comprising a total of 687 HL patients, ^{18}F-FDG-PET/CT was found superior to BMB in detecting BMI. Pooled sensitivity of ^{18}F-FDG-PET/CT was determined as 94.5% [95% confidence interval (CI): 89.0-97.8%] whereas the corresponding estimate for BMB was 39.4% (95% CI: 30.8-48.8%).

In the study by Adams et al. (13) on 26 newly diagnosed HL patients, visual ^{18}F-FDG-PET/CT results were compared to BMB of the right iliac crest, which is used as the gold standard method. Accordingly, ^{18}F-FDG-PET/CT was found to be 100% sensitive (95% CI: 51.1-100%), 100% specific (95% CI: 81.8-100%) in detecting BMI with 100% (95% CI: 51.1-100%) PPV, 100% (95% CI: 81.8-100%) NPV. Additionally, SUV_{max} of BMB positive patients [mean±standard deviation (SD): 3.4±0.85] was higher than that of BMB negative patients almost reaching statistical significance (mean±SD 2.7±0.63) (p=0.052) (13).

In our study, 64 of the 172 patients were diagnosed with HL. Concordance between BMB and ^{18}F-FDG-PET/CT was observed in 50 (78%) of the 64 patients. Among these 50 cases, both tests were negative in 46 and positive in 4. In the remaining 14 patients, 13 were ^{18}F-FDG-PET/CT positive, BMB negative and one patient was BMB positive without any involvement on ^{18}F-FDG-PET/CT. Thus, considering BMB as the gold standard, ^{18}F-FDG-PET/CT was found to be 80% sensitive, 78% specific for detecting BMI with 24% PPV and 98% NPV. The high sensitivity and specificity values were consistent with the literature. On semi-quantitative assessment, there was no significant difference in SUV_{max} values between BMB positive and negative cases among the PET/CT positive patients. Additionally, in our study, AUC and cut-off values for HL patients were found as 0.7763 and 4, respectively.

Similar studies on NHL patients are also available in the literature. In the study by Muslimani et al. (14), 97 NHL patients were grouped according to the presence of low or high grade disease, and the results of ^{18}F-FDG-PET/CT scan for initial staging and unilateral iliac crest BMB were compared. Unlike other studies in the literature, samples were obtained from the involvement sites in BMB-negative patients with ^{18}F-FDG-PET/CT images suggesting BMI. Consequently, BMB from sites of involvement of the 11 patients who were initially BMB-negative and ^{18}F-FDG-PET/CT positive, revealed 6 positive BMB results. Positive repeat biopsies were obtained from the contralateral iliac crest in 1, from the humerus in 2, from the tibia in 1 and from the fourth vertebra in one patient. Thus, ^{18}F-FDG-PET/CT was 79% sensitive, 91% specific for detecting BMI with 87% PPV and 87% NPV. Additionally, there was no significant difference between the low and high grade NHL groups in terms of the ability of ^{18}F-FDG-PET to detect BMI (sensitivity p=0.23, specificity p=0.64). In conclusion, the high potential of ^{18}F-FDG-PET in detecting BMI in NHL was highlighted and BMB sampling was recommended for BMB negative patients whose ^{18}F-FDG-PET scan demonstrates BM involvement (14). In our study, biopsies were obtained only from the iliac crest and not from other sites observed positive on PET/CT, which is a limitation of our study. We could have found higher sensitivity and specificity values if

biopsy sampling was done from sites other than the iliac crest in cases who were biopsy negative. Many studies in the literature have reported that in the majority of BMB-negative cases multifocal involvement was observed on ^{18}F-FDG-PET/CT and that biopsies obtained from the sites of involvement were almost always positive (5,15,16,17).

In our study, among the 33 cases with infiltration on PET/CT, 11 had diffuse heterogeneous patchy accumulations. Diffuse accumulations may be secondary to benign conditions such as inflammation, thus some studies (13) have excluded such cases while others have not (11). In our study diffuse accumulations were heterogeneous and patchy, thus they were included since they were not homogenous lesions.

In the study by Lee et al. (18), 120 high grade NHL patients comprised of newly diagnosed DLBCL and peripheral T-cell lymphoma cases were included to assess the role of ^{18}F-FDG-PET/CT in the detection of BMI. Bilateral iliac crest BMB results were considered the gold standard. ^{18}F-FDG-PET/CT and BMB results were concordant in 100 of the 120 patients (both positive or negative) while 20 were non-concordant. Besides, SUV_{max} values of patients demonstrating abnormal ^{18}F-FDG accumulation were significantly higher as compared to those with normal ^{18}F-FDG accumulation. It was concluded that ^{18}F-FDG-PET/CT and BMB are complementary techniques in assessing BMI in patients with high-grade lymphomas, and obtaining biopsies from sites of accumulation was recommended for patients showing ^{18}F-FDG-avidity although standard iliac crest BMB are negative (18).

Berthet et al. (19) evaluated ^{18}F-FDG-PET/CT performance for detecting BMI with reference to BMB and its effect on progression-free/overall survival in their study on 142 patients with DLBCL. In case of negative BMB, ^{18}F-FDG-PET/CT accumulation areas were evaluated by biopsy or MR images. Accordingly, as compared to BMB, ^{18}F-FDG-PET/CT had significantly higher sensitivity (94% vs. 24%, p<0.001), NPV (98% vs. 80%) and accuracy (98% vs. 81%). Multivariate analysis showed that BMI detected by ^{18}F-FDG-PET/CT was an independent predictor of progression-free survival (PFS) (p=0.02) but not for overall survival. It was concluded that, assessment of BMI with ^{18}F-FDG-PET/CT has higher diagnostic and prognostic prediction in newly diagnosed DLBCL patients as compared to BMB (19).

Zhou et al. (20) evaluated the role of ^{18}F-FDG-PET/CT in detecting BMI and compared overall (OS) and PFS rates of patients who were concordantly negative (PET-CT/BMB-) or positive (PET-CT/BMB+) in 55 patients with newly diagnosed extranodal natural killer/T cell lymphoma. Using BMB results as reference, the study found the sensitivity and specificity rates of ^{18}F-FDG-PET/CT for detecting BMI as 100% and 86%, respectively. Following the median follow-up period of 16 months (range, 3-43 months) PET-CT/BMB positive patient group showed worsened 2-year OS as compared to PET-CT/BMB negative group (84.8% vs. 67.9%, p<0.05). On the other hand, the estimated 2-year PFS rates for PET-CT/BMB negative and PET-CT/BMB positive patients were 72.7% and 41.9%, respectively. However, it was concluded that, due to the small number of PET-CT/BMB positive patients, it would be incorrect to conclude that survival rates were similar for both groups in advanced stage patients. Finally, the prognostic and complementary diagnostic role of ^{18}F-FDG-PET/CT in detecting BMI, especially in cases missed by BMB, was underlined (20).

In our study, 108 of the 172 patients had NHL diagnosis and among these 16 (14.8%) were ^{18}F-FDG-PET/CT positive and 37 (34.2%) were BMB positive. Subtyping/grading was not performed for NHL patient group. Concordance between the two tests was observed in 73 (67%) patients; 64 patients were PET-CT/BMB negative while 9 patients were PET-CT/BMB positive. Non-concordance was observed in 35 patients; of which 7 were ^{18}F-FDG-PET/CT positive, BMB negative and the remaining 28 patients were BMB positive, ^{18}F-FDG-PET/CT negative. As a result, ^{18}F-FDG-PET/CT was found to be 24% sensitive, 90% specific for detecting BMI with PPV 56% and NPV 70%. We suggest that the low sensitivity for the NHL subgroup may be due to the lack of histological subgrouping in this patient group. Studies have reported higher ^{18}F-FDG-PET/CT sensitivity rates in detecting BMI in aggressive NHL subtypes, while 2/3 false negativity ratio was observed in indolent histological forms (e.g., grade 1 and 2 follicular lymphomas) leading to lower sensitivity values (9). Additionally, in our study, AUC and cut-off values for NHL patients were found as 0.6534 and 3.2, respectively.

Conclusion

In this study, a moderately high concordance (71%) was observed between PET/CT and BMB findings. The rate of concordance was higher in HL patients (78%) as compared to NHL patients (67%). In conclusion, PET/CT appears to be a significant method for detecting BM infiltration in comparison to BM biopsy which is an invasive method. Currently, BM biopsy is usually performed from the iliac crest while PET/CT has the advantage of whole body imaging to allow for detection of involvement sites other than the iliac bone. In this regard, although PET/CT is not a substitute for BM biopsy, we suggest that it can be used as a guide to biopsy site and a complementary imaging technique for BM biopsy.

Ethics

Ethics Committee Approval: The study was approved by the Akdeniz University Local Ethics Committee (date: 21.01.2015) (protocol number: 35), **Informed Consent:** Consent form was filled out by all participants.

Peer-review: Externally peer-reviewed.

Authorship Contributions

Surgical and Medical Practices: O.S., O.K.Y., L.U., Concept: A.O.Ö., E.S.B., F.A., Design: A.O.Ö., E.S.B., F.A., Data Collection or Processing: A.O.Ö., F.A., B.A., O.S., Analysis or Interpretation: A.O.Ö., F.A., T.T., A.B., A.Y., F.G., Literature Search: A.O.Ö., E.S.B., Writing: A.O.Ö., E.S.B., F.A.

Conflict of Interest: No conflict of interest was declared by the authors.

Financial Disclosure: The authors declared that this study received no financial support.

References

1. Pelosi E, Penna D, Deandreis D, Chiappella A, Skanjeti A, Vitolo U, Bisi G. FDG-PET in the detection of bone marrow disease in Hodgkin's disease and aggressive non-Hodgkin's lymphoma and its impact on clinical management. Q J Nucl Med Mol Imaging 2008;52:9-16.
2. Stumpe KD, Urbinelli M, Steinert HC, Glanzmann C, Buck A, von Schulthess GK. Whole-body positron emission tomography using fluorodeoxyglucose for staging of lymphoma: effectiveness and comparison with computed tomography. Eur J Nucl Med 1998;25:721-728.
3. Brusamolino E, Bacigalupo A, Barosi G, Biti G, Gobbi PG, Levis A, Marchetti M, Santoro A, Zinzani PL, Tura S. Classical Hodgkin's lymphoma in adults: guidelines of the Italian Society of Hematology, the Italian Society of Experimental Hematology, and the Italian Group for Bone Marrow Transplantation on initial work-up, management, and follow-up. Haematologica 2009;94:550-565.
4. Howell SJ, Grey M, Chang J, Morgenstern GR, Cowan RA, Deakin DP, Radford JA. The value of bone marrow examination in the staging of Hodgkin's lymphoma: a review of 955 cases seen in a regional cancer centre. Br J Haematol 2002;119:408-411.
5. Moulin-Romsee G, Hindié E, Cuenca X, Brice P, Decaudin D, Bénamor M, Brière J, Anitei M, Filmont JE, Sibon D, de Kerviler E, Moretti JL. 18F-FDG-PET/CT bone/bone marrow findings in Hodgkin's lymphoma may circumvent the use of bone marrow trephine biopsy at diagnosis staging. Eur J Nucl Med Mol Imaging 2010;37:1095-1105.
6. Buchmann I, Moog F, Schirrmeister H, Reske SN. Positron emission tomography for detection and staging of malignant lymphoma. Recent Results Cancer Res 2000;156:78-89.
7. Kostakoglu L, Coleman M, Leonard JP, Kuji I, Zoe H, Goldsmith SJ. PET predicts prognosis after 1 cycle of chemotherapy in aggressive lymphoma and Hodgkin's disease. J Nucl Med 2002;43:1018-27.
8. Moog F, Bangerter M, Kotzerke J, Guhlmann A, Frickhofen N, Reske SN. 18-F-fluorodeoxyglucose-positron emission tomography as a new approach to detect lymphomatous bone marrow. J Clin Oncol 1998;16:603-609.
9. Fuster D, Chiang S, Andreadis C, Guan L, Zhuang H, Schuster S, Alavi A. Can [18F]fluorodeoxyglucose positron emission tomography imaging complement biopsy results from the iliac crest for the detection of bone marrow involvement in patients with malignant lymphoma? Nucl Med Commun 2006;27:11-15.
10. Cortés-Romera M, Sabaté-Llobera A, Mercadal-Vilchez S, Climent-Esteller F, Serrano-Maestro A, Gámez-Cenzano C, Gonzalez-Barca E. Bone marrow evaluation in initial staging of lymphoma: 18F-FDG-PET/CT versus bone marrow biopsy. Clin Nucl Med 2014;39:46-52.
11. Muzahir S, Mian M, Munir I, Nawaz MK, Faruqui ZS, Mufti KA, Bashir H, Uddin N, Siddiqui N, Maaz AU, Mahmood MT. Clinical utility of 18F FDG-PET/CT in the detection of bone marrow disease in Hodgkin's lymphoma. Br J Radiol 2012;85:490-496.
12. Cheng G, Alavi A. Value of 18F-FDG-PET versus iliac biopsy in the initial evaluation of bone marrow infiltration in the case of Hodgkin's disease: a meta-analysis. Nucl Med Commun 2013;34:25-31.
13. Adams HJ, Kwee TC, Fijnheer R, Dubois SV, Nievelstein RA, de Klerk JM. Bone marrow FDG-PET/CT in Hodgkin lymphoma revisited: do imaging and pathology match? Ann Nucl Med 2015;29:132-137.
14. Muslimani AA, Farag HL, Francis S, Spiro TP, Chaudhry AA, Chan VC, Taylor HC, Daw HA. The utility of 18-F-fluorodeoxyglucose positron emission tomography in evaluation of bone marrow involvement by non-Hodgkin lymphoma. Am J Clin Oncol 2008;31:409-412.
15. Cheng G, Chen W, Chamroonrat W, Torigian DA, Zhuang H, Alavi A. Biopsy versus FDG-PET/CT in the initial evaluation of bone marrow involvement in pediatric lymphoma patients. Eur J Nucl Med Mol Imaging 2011;38:1469-1476.
16. Ribrag V, Vanel D, Leboulleux S, Lumbroso J, Couanet D, Bonniaud G, Aupérin A, Masson F, Bosq J, Edeline V, Fermé C, Pigneur F, Schlumberger M. Prospective study of bone marrow infiltration in aggressive lymphoma by three independent methods: whole-body MRI, PET/CT and bone marrow biopsy. Eur J Radiol 2008;66:325-331.
17. Purz S, Mauz-Körholz C, Körholz D, Hasenclever D, Krausse A, Sorge I, Ruschke K, Stiefel M, Amthauer H, Schober O, Kranert WT, Weber WA, Haberkorn U, Hundsdörfer P, Ehlert K, Becker M, Rössler J, Kulozik AE, Sabri O, Kluge R. [18F]Fluorodeoxyglucose positron emission tomography for detection of bone marrow involvement in children and adolescents with Hodgkin's lymphoma. J Clin Oncol 2011;29:3523-3528.
18. Lee Y, Hwang KH, Hong J, Park J, Lee JH, Ahn JY, Kim JH, Lee H, Kim SG, Shin JY. Usefulness of (18)F-FDG-PET/CT for the Evaluation of Bone Marrow Involvement in Patients with High-Grade Non-Hodgkin's Lymphoma. Nucl Med Mol Imaging 2012;46:269-277.
19. Berthet L, Cochet A, Kanoun S, Berriolo-Riedinger A, Humbert O, Toubeau M, Dygai-Cochet I, Legouge C, Casasnovas O. In newly diagnosed diffuse large B-cell lymphoma, determination of bone marrow involvement with 18F-FDG-PET/CT provides better diagnostic performance and prognostic stratification than does biopsy. J Nucl Med 2013;54:1244-1250.
20. Zhou Z, Chen C, Li X, Li Z, Zhang X, Chang Y, Lu L, Cui Y, Ma Y, Zhang M. Evaluation of bone marrow involvement in extranodal NK/T cell lymphoma by FDG-PET/CT. Ann Hematol 2015;94:963-967.

Original Article
Mol Imaging Radionucl Ther 2017;26:76-82 DOI:10.4274/mirt.07769

Clinical Significance of ^{18}F-Fluorodeoxyglucose Avid Prostate Gland Incidentalomas on Positron Emission Tomography/Computed Tomography

Pozitron Emisyon Tomografisi/Bilgisayarlı Tomografide ^{18}F-Fluorodeoksiglukoz Avid Prostat Bezi İnsidentalomalarının Klinik Önemi

William Makis[1], Anthony Ciarallo[2]
[1]Cross Cancer Institute, Department of Diagnostic Imaging, Edmonton, Canada
[2]McGill University Health Centre Glen Site, Department of Nuclear Medicine, Montreal, Canada

Abstract

Objective: The aim of this study was to evaluate the clinical significance of incidental focal uptake of ^{18}F-fluorodeoxyglucose (^{18}F-FDG) on positron emission tomography/computed tomography (PET/CT) in the prostate glands of cancer patients.

Methods: A retrospective review of 3122 consecutive male patients who underwent ^{18}F-FDG PET/CT studies with an oncologic indication, over the course of four years, was performed. Studies with incidental ^{18}F-FDG uptake in the prostate gland were further analyzed.

Results: Incidental ^{18}F-FDG uptake in the prostate gland was identified in 65/3122 men (2.1%). Sufficient follow-up data (≥12 months) were available in 53 patients, of whom 11 had a biopsy and 42 had clinical and imaging follow-up. Malignancy was histologically diagnosed in 4 out of 53 patients (7.5%). There was no statistically significant difference in ^{18}F-FDG uptake values between benign prostate lesions [maximum standardized uptake value (SUV_{max}) 7.3] and malignant ones (SUV_{max} 7.2, p=0.95). There was a statistically significant difference between the serum prostate specific antigen (PSA) of the benign group (n=24, PSA=2.7 ng/mL) and the malignant group (n=4, PSA=9.2 ng/mL, p<0.001). There was a direct correlation between SUV_{max} and Gleason score.

Conclusion: ^{18}F-FDG positive prostate incidentalomas were detected in 2.1% of oncologic PET/CT scans and of these 7.5% were malignant. SUV_{max} was not useful for distinguishing between benign and malignant incidental prostate lesions. ^{18}F-FDG avid prostate incidentalomas on PET/CT should prompt a recommendation for obtaining a serum PSA and further investigation if serum PSA is elevated.

Keywords: Prostate incidentaloma, prostate carcinoma, ^{18}F-fluorodeoxyglucose, positron emission tomography/computed tomography, prostate specific antigen

Öz

Amaç: Bu çalışmanın amacı kanser hastalarının prostat bezinde pozitron emisyon tomografisi/bilgisayarlı tomografide (PET/BT) insidental olarak saptanan fokal ^{18}F-fluorodeoksiglukoz (^{18}F-FDG) tutulumunun klinik önemini değerlendirmektir.

Yöntem: Dört yıllık bir dönemde onkolojik nedenlerle ^{18}F-FDG-PET/BT uygulanmış 3122 ardışık erkek hasta retrospektif olarak incelendi. Prostat bezinde insidental ^{18}F-FDG tutulumu saptanan hastalar detaylı olarak değerlendirildi.

Address for Correspondence: William Makis MD, Cross Cancer Institute, Department of Diagnostic Imaging, Edmonton, Canada
Phone: 7804328760 E-mail: makisw79@yahoo.com **Received:** 14.01.2017 **Accepted:** 16.02.2017

Öz

Bulgular: Prostat bezinde insidental ^{18}F-FDG tutulumu 65/3,122 erkekte (%2,1) saptandı. Yeterli takip verisi (≥12 ay) olan 53 hasta mevcuttu, bunların 11'ine biyopsi uygulanmış 42'si klinik ve radyolojik olarak takip edilmişti. Elli üç hastanın dördünde malignite histolojik olarak saptanmıştı (%7,5). Benign ve malign prostat lezyonlarında ^{18}F-FDG tutulum değerleri açısından istatistik olarak anlamlı fark yoktu [maksimum standart uptake değeri (SUV_{maks}) benign: SUV_{maks} 7,3, malign: SUV_{maks} 7,2, p=0,95]. Benign ve malign grup hastalarda serum prostat spesifik antijen (PSA) değerleri arasında istatistiksel olarak anlamlı fark vardı (benign grup n=24, PSA=2,7 ng/mL, malign grup n=4, PSA=9,2 ng/mL, p<0,001). SUV_{max} ve Gleason skoru arasında direkt korelasyon mevcuttu.

Sonuç: Onkolojik PET/BT görüntülemelerinin %2,1'inde ^{18}F-FDG pozitif prostat bezi insidentaloması saptandı ve bunların %7,5'i malign idi. SUV_{maks}, benign ve malign insidental prostat lezyonlarını ayırt etmede yararlı değildi. PET/BT'de ^{18}F-FDG tutulumu olan prostat bezi insidentaloması varlığında serum PSA değerinin bakılması önerilmeli ve eğer PSA yüksek ise ileri tetkik gerekliliği akılda tutulmalıdır.

Anahtar kelimeler: Prostat bezi insidentaloması, prostat kanseri, ^{18}F-fluorodeoksiglukoz, pozitron emisyon tomografisi/bilgisayarlı tomografi, prostat spesifik antijen

Introduction

Since positron emission tomography/computed tomography (PET/CT) was first introduced for the staging and follow-up of various malignancies, PET/CT readers have been faced with the challenge of interpreting foci of increased ^{18}F-fluorodeoxyglucose (^{18}F-FDG) uptake in unexpected locations. In addition to malignancy, ^{18}F-FDG uptake has been described in various sites of normal physiologic processes and tracer biodistribution, in benign nodules and masses, and in infectious and inflammatory processes (1,2,3). Increased ^{18}F-FDG activity in locations not typical for metastatic spread in patients known for malignancy may alternatively represent an unrelated benign process or even a second primary malignancy, thus complicating the interpretation of the PET/CT study. The most common locations of potentially malignant incidental ^{18}F-FDG uptake reported in the literature include: breast, gastrointestinal system, the prostate, thyroid, adrenal and parotid glands (4,5,6,7,8,9,10). Locations such as the thyroid, adrenal, and gastrointestinal system have been investigated extensively in the literature, while locations such as the prostate gland continue to confound PET/CT readers.

Several studies have investigated the clinical significance of ^{18}F-FDG positive prostate incidentalomas (11,12,13,14,15,16,17). The aim of this study was to determine the frequency of unexpected focal uptake of ^{18}F-FDG on PET/CT in the prostate glands of cancer patients and to detect the proportion of malignant cases within this group. We examined the possibility of using standardized uptake value (SUV_{max}) to differentiate benign causes of incidental prostate ^{18}F-FDG uptake from malignant ones. We also examined if serum prostate specific antigen (PSA) values were different in the benign group as compared to the malignant group.

Materials and Methods

Study Design and Patient Population

3122 consecutive male patients who underwent ^{18}F-FDG PET/CT studies with an oncologic indication over the course of 48 months (from January 1, 2006 to December 31, 2009) were retrospectively reviewed at our institution, a tertiary care academic hospital. The PET/CT reports that made a special reference to focal ^{18}F-FDG uptake in the prostate gland provided the basis for this study.

Sixty-five patients had incidental ^{18}F-FDG uptake in the prostate gland and represented the study group. Patients with a previous prostate malignancy or prostatectomy (n=3) were excluded from the study. Patients with insufficient follow-up data (<12 months) (n=9) were also excluded from this study. The remaining 53 cases constituted the study group for further assessment of clinical significance of incidental ^{18}F-FDG uptake in the prostate gland.

Positron Emission Tomography/Computed Tomography Imaging

^{18}F-FDG PET/CT studies were performed on a hybrid PET/CT scanner (Discovery ST, General Electric Medical Systems, Waukesha, WI, USA), which combines a dedicated, full-ring PET scanner with a 16-slice CT scanner. Patients were required to fast for at least 6 hours before the time of their appointment, and waited in a quiet dark room the morning of their scan. Blood glucose levels were recorded immediately prior to ^{18}F-FDG administration. If the serum glucose level was greater than 11.1 mmol/L (200 mg/dL), the study was rescheduled. A volume of 400 mL of barium sulfate oral contrast was administered, and 8.14 MBq/kg of ^{18}F-FDG was injected intravenously up to a maximum dose of 740 MBq. Approximately sixty minutes following ^{18}F-FDG injection, CT and PET images were consecutively acquired from the base of the skull to the upper thighs, with

additional images of the extremities acquired if needed. CT scan settings were: 140 kVp, 90-110 mA (depending on the body weight), a rotation time of 0.8 s, a table speed of 17 mm per gantry rotation, a pitch of 1.75:1, and a detector row configuration of 16×0.625 mm. For the PET portion of the study, a 2-D acquisition was performed and images were acquired for 4-5 min per bed position (depending on the body weight) up to 5 to 6 total bed positions (depending on the patient's height). The patient was allowed to breathe normally during the PET and CT acquisitions.

Data obtained from the CT acquisition were used for attenuation correction and fusion with PET images. The PET data were reconstructed iteratively using ordered subset expectation maximization software provided by the manufacturer (21 subsets, 2 iterations). PET attenuation corrected, PET non-attenuation corrected, CT, and PET/CT fusion images of the whole body were displayed in the transaxial, coronal, and sagittal planes and were reviewed on a dedicated workstation (Xeleris 2.0, GE Healthcare, Waukesha, WI, USA). PET data were also displayed in a rotating maximum intensity projection image.

Interpretation and Analysis of Positron Emission Tomography/Computed Tomography Images

All PET/CT images were interpreted using visualization and semi-quantitative analysis (SUV_{max} corrected for body weight) by two experienced nuclear physicians, independently. Any focal ^{18}F-FDG uptake in the prostate gland was noted and each nuclear medicine physician measured the SUV_{max} corrected for body weight, using a spherical region of interest at the site of the most intense uptake in the prostate gland.

Diagnosis and Follow-up

Final diagnosis of benign or malignant prostate incidentaloma was based on histologic tissue sampling in 11 of 53 patients. The remaining 42 patients were assessed clinically and/or by serial imaging with magnetic resonance imaging (MRI) or PET/CT. Lesions were considered benign on serial imaging if there was no further evidence of malignancy in the prostate gland or if there was evidence of regression in SUV_{max} by at least 50% in the absence of treatment over a period of at least 12 months. Serum PSA values obtained within 6 months of the PET/CT scan were compared in the benign and malignant groups.

Statistical Analysis

The Mann-Whitney U test was used to determine if there was a significant difference between the mean SUV_{max} values of the benign and malignant groups. The Mann-Whitney U (two tailed) test was used to detect a significant difference between the serum PSA values of the benign and malignant groups. A p value less than 0.05 was considered to indicate a statistically significant difference. A correlation between Gleason score and SUV_{max} was established using the Spearman's rank correlation coefficient.

Results

The mean age of the study group was 69.3 years (range: 45-87 years). The primary malignant tumors of the cohort and their relative distribution are listed below (Table 1). Incidental focal ^{18}F-FDG uptake in the prostate gland was found in 65 of 3122 (2.1%) men scanned consecutively with PET/CT for an oncologic indication. The mean age of patients with benign prostate lesions was 68.8 years as compared to 74.0 years in patients with prostate malignancy. The distribution of abnormal ^{18}F-FDG prostate uptake in the 53 patients with sufficient follow-up were identified as: peripheral n=37 (69.8%), central n=7 (13.2%), and multifocal or heterogeneous n=9 (17.0%) (Table 2).

Histologic tissue sampling was available in 11 of 53 patients, and the remaining 42 patients were assessed clinically and/or by serial imaging with MRI or PET/CT. The mean clinical follow-up period of these 42 patients was 33 months (range: 12-66 months). Out of 53 patients, 49 (92.5%)

Table 1. Characteristics of the cohort

Demographics	(n=53)
Age (years), mean (SD)	69.3 (9.7)
Age (years), median (IQR)	69.0 (64; 76)
Indication, n (%)	
Rectal cancer	17 (32.1)
Lymphoma	8 (15.1)
Colon cancer	6 (11.3)
Lung cancer	6 (11.3)
Malignancy work-up	5 (9.4)
GIST	3 (5.7)
Hepatocellular cancer	2 (3.8)
Bladder cancer	2 (3.8)
Brain lesion	1 (1.9)
Cholangiocarcinoma	1 (1.9)
Gastric cancer	1 (1.9)
Penile cancer	1 (1.9)

SD: Standard deviation, IQR: Interquartile range, GIST: Gastrointestinal stromal tumor

Table 2. Distribution of prostate ^{18}F-fluorodeoxyglucose uptake

Site	n (%)	Cancer
Peripheral	37 (69.8)	4
Central	7 (13.2)	0
Heterogeneous	9 (17.0)	0

were diagnosed with a benign prostate process and 4 (7.5%) were diagnosed with prostate adenocarcinoma. There was no statistically significant difference in terms of the mean SUV_{max} values between the benign (SUV_{max} 7.3) and the malignant group (SUV_{max} 7.2) (p value 0.95, Mann-Whitney U test) (Table 3). The four malignant prostate incidentalomas were identified in patients with various primary malignancies and all four malignant cases had ^{18}F-FDG uptake in the peripheral zone of the prostate gland (Table 4). The SUV_{max} range of the four malignant cases was 4.7-9.9, while the SUV_{max} range of the seven benign biopsied cases was 2.1-22.0, with histology evaluation showing two cases of benign prostatic hyperplasia (BPH) and five cases of benign prostate tissue (Table 5).

Serum PSA values obtained within 6 months of the PET/CT were available in 28 of 53 (52.8%) patients. Of those patients with available serum PSA values, 24 of 28 (85.7%) were diagnosed as benign and 4 of 28 (14.3%) were diagnosed as malignant. Mean serum PSA value of patients with a benign prostate process was 2.7 ng/mL versus 9.2 ng/mL for patients with a malignant prostate incidentaloma, a statistically significant difference with a p value <0.001 by Mann-Whitney U test (Figure 1). The lowest PSA value of the malignant cases was 6.7 ng/mL.

The Gleason scores of the malignant prostate incidentalomas correlated directly with SUV_{max} (Spearman's rank coefficient, rho=0.996, p=0.004) (Figure 2).

Discussion

In our study, 2.1% of PET/CT scans performed in men with an oncologic indication revealed incidental uptake in the prostate gland, in keeping with previously reported values ranging from 0.6% to 4.5% (11,12,13,14,15,16,17). However, the incidence of ^{18}F-FDG positive prostate incidentalomas that have been confirmed to be malignant varies widely in the literature, from 5.4% (11) up to 58.0% (13), making it difficult for the interpreting physician to

Table 3. Benign vs. malignant prostate lesions

	Benign (n=49)	Malignant (n=4)	p value
Age (y), mean (SD)	68.8 (9.9)	74.0 (6.8)	0.32
SUV_{max}, mean (SD)	7.3 (5.3)	7.2 (2.5)	0.95
SUV_{max}, range (min.; max.)	(2.1; 27.0)	(4.7; 9.9)	-
	Benign (n=24)	**Malignant (n=4)**	
PSA, mean (SD)	2.7 (2.0)	9.2 (3.1)	0.001
PSA, range (min.; max.)	0.3-8.9	6.7-13.6	-

SD: Standard deviation, Min.: Minimum, Max.: Maximum, SUV_{max}: Maximum standardized uptake value, PSA: Prostate specific antigen

Table 4. Biopsied malignant prostate incidentalomas

Patient	Age	Primary	SUV_{max}	Site	PSA (ng/mL)	Gleason
1	65	GIST	9.9	Peripheral	7.4	10 (5+5)
2	81	Lymphoma	8.5	Peripheral	13.6	9 (4+5)
3	73	Cholangioca	5.5	Peripheral	6.7	7 (3+4)
4	77	Rectal cancer	4.7	Peripheral	8.9	6 (3+3)

GIST: Gastrointestinal stromal tumor, SUV_{max}: Maximum standardized uptake value, PSA: Prostate specific antigen

Table 5. Biopsied benign prostate incidentalomas

Patient	Age	Primary	SUV_{max}	Site	PSA (ng/mL)	Histology
5	67	Rectal cancer	22.0	Peripheral	4.1	Benign
6	68	Lung cancer	16.2	Central	4.2	Benign
7	72	Bladder cancer	6.4	Heterogen	4.1	BPH
8	58	Lymphoma	4.4	Peripheral	2.0	Benign
9	64	Gastric cancer	3.7	Heterogen	N/A	Benign
10	73	Lymphoma	3.2	Peripheral	N/A	Benign
11	80	Colon cancer	2.1	Peripheral	8.9	BPH

Note: BPH-benign prostatic hyperplasia, benign-benign prostate tissue, heterogen-heterogeneous, SUV_{max}: Maximum standardized uptake value, PSA: Prostate specific antigen

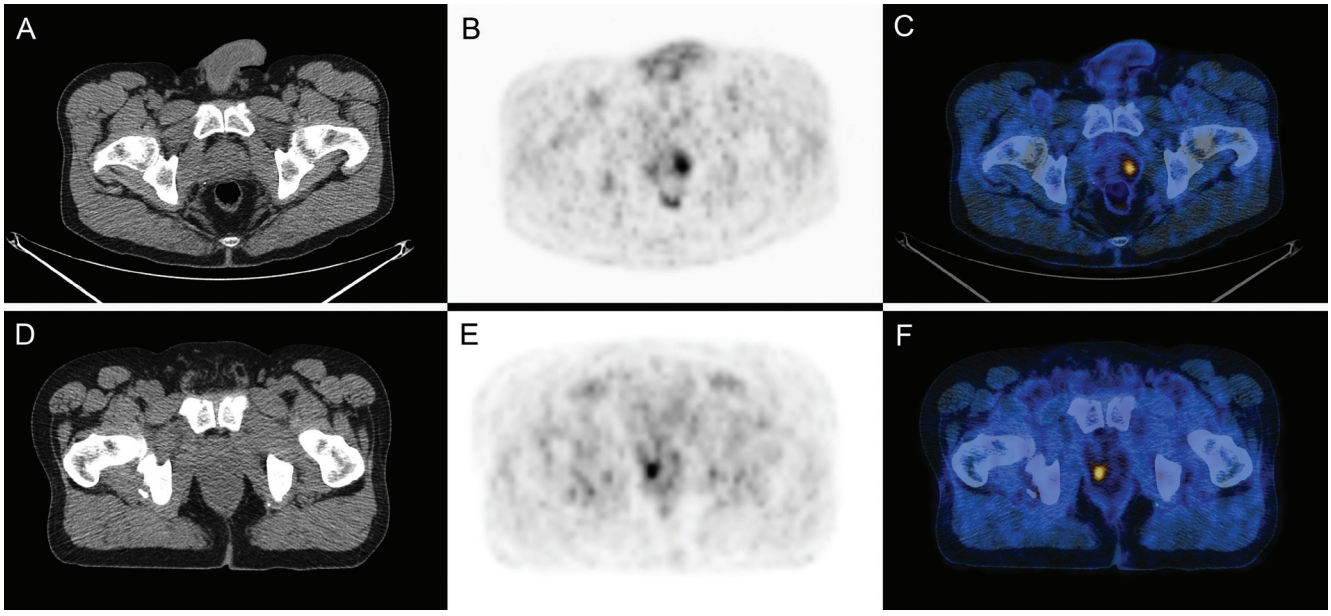

Figure 1. Two histologically confirmed cases of ^{18}F-fluorodeoxyglucose (^{18}F-FDG) positive prostate incidentaloma, one benign and one malignant, with similar maximum standardized uptake value (SUV_{max}) values. A 58 year old man with previous history of Hodgkin lymphoma (Table 5, patient 8) had a follow-up ^{18}F-FDG positron emission tomography/computed tomography (PET/CT). A serum prostate specific antigen done within 6 months of the PET/CT was 2.0 ng/mL and a biopsy of the prostate did not reveal any malignancy, only benign prostate tissue. A, B, C) Axial PET/CT images show a focus of intense ^{18}F-FDG uptake in the prostate with SUV_{max} 4.4, consistent with a false positive. A 77 year old man with a previous history of rectal cancer (Table 4, patient 4) had a follow-up ^{18}F-FDG-PET/CT. A serum prostate specific antigen done within 1 month was 8.9 ng/mL and biopsy of the prostate showed prostate carcinoma with Gleason score 6 (3+3). D, E, F) Axial PET/CT images show a focus of ^{18}F-FDG uptake in the prostate with SUV_{max} 4.7, consistent with a true positive

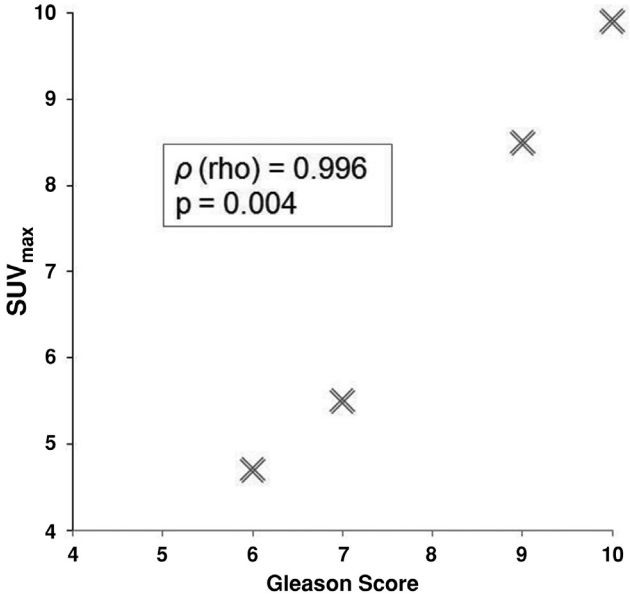

Figure 2. The Gleason scores of the malignant prostate incidentalomas correlated directly with maximum standardized uptake value (Spearman's rank coefficient, rho=0.996, p=0.004)
SUV_{max}: Maximum standardized uptake value

decide what to report or recommend when faced with this uncommon incidental PET/CT finding. In our patient population, 7.5% (4 of 53) of ^{18}F-FDG positive prostate incidentalomas were malignant. There was no particular cancer population which seemed to be at a higher risk of incidental prostate cancer. These findings are similar to those reported by Han et al. (11), who reported prostate malignancy in 5.4% of 55 incidentalomas. It is important to note that in most prostate incidentaloma papers, a significant number of prostate incidentalomas have not been investigated further and do not have any long term follow-up, likely resulting in an overestimation of reported malignancy rates. Only studies by Han et al. (11) and Seino et al. (15) evaluated most of their prostate incidentalomas [87% 55/63 by Han et al. (11), 92% 49/53 by Seino et al. (15)]. Neither of these studies had long term follow-up of their benign prostate incidentalomas. Our mean follow-up period for benign prostate incidentalomas was 33 months.

All prostate incidentaloma studies published thus far confirm that quantitative analysis using SUV_{max} values alone cannot differentiate benign incidental prostate lesions from malignant ones. Similarly, our data failed to demonstrate a statistically significant difference between mean SUV_{max} values for the benign and malignant groups. High SUV_{max} values have been reported in several benign prostate conditions such as prostatitis (18), BPH (19), as well as other malignant

prostate conditions (20,21,22,23), such as seminoma (20), sarcomatoid carcinoma (21), and neuroendocrine tumor of the prostate (22). If clinical significance of an ^{18}F-FDG positive prostate incidentaloma is to be determined, it requires more information than SUV_{max} alone.

Prostate cancer is often confirmed by histological examination of a sample obtained by needle biopsy. However, this intervention is invasive and unnecessary in the vast majority of patients with ^{18}F-FDG positive prostate incidentalomas. PSA and digital rectal examination are useful non-invasive screening tests routinely used in clinical practice (24,25,26,27,28,29,30). In our population, there was a statistically significant difference between the serum PSA values of benign prostate incidentalomas (n=24, PSA=2.7 ng/mL) and malignant prostate incidentalomas (n=4, PSA=9.2 ng/mL, $p<0.001$), which is in keeping with the majority of published studies on ^{18}F-FDG avid prostate incidentalomas (11,12,13,14,15,16,17).

Some investigators have noted a statistically significant association between SUV_{max} and Gleason score, whereby prostate lesions with higher Gleason scores also had higher SUV_{max} values on PET/CT (31,32). Our study found a direct correlation between Gleason score and SUV_{max} in malignant prostate incidentaloma cases. Even though most ^{18}F-FDG positive prostate incidentalomas are statistically benign, a markedly elevated SUV_{max} arguably warrants closer follow up in these patients to avoid missing an aggressive malignancy.

There are several limitations to our study. Although the minimum follow-up time was set at 12 months, and the mean period of clinical follow-up of 42 prostate incidentalomas who did not have a biopsy was 33 months, longer follow-up would likely improve the results, especially due to the indolent nature of prostate cancer. Another limitation was that serum PSA values were not obtained in all prostate incidentaloma patients, and the timing of obtained PSA values ranged from the same day of to up to 6 months within the PET/CT. Ideally, serum PSA values should be available in all patients with prostate incidentalomas and performed at the same time as the PET/CT.

Several PSA related indices, such as free-to-total PSA ratio (F/T ratio), PSA density (PSAD) and PSA transition zone density (PSATZ) could further improve the differentiation of benign ^{18}F-FDG positive prostate incidentalomas from malignant ones. These indices appear to improve cancer detection sensitivity and specificity in patients with low serum PSA levels. The ratio of free-to-total PSA (F/T ratio) is known to be reduced in cases of prostate cancer. For patients with PSA levels between 4.0 and 10.0 ng/mL, the recommended cut-off value for F/T is ≤0.25. The ideal cut-off for PSAD is 0.15 ng/mL/cm^3 (26,27,28,29,30). These indices may one day play a role in helping determine whether a patient with an ^{18}F-FDG positive prostate incidentaloma is at high risk for harboring a prostate malignancy and should have a biopsy or whether a biopsy is not necessary. Novel PET/CT agents such as gallium-68 (^{68}Ga)- prostate-specific membrane antigen (PSMA) may also become useful in differentiating benign ^{18}F-FDG avid prostate incidentalomas from malignant ones, as several studies have recently reported prostate cancer detection rates by ^{68}Ga-PSMA PET/CT imaging in the range of 90-100% (33,34,35).

Conclusion

In our patient population, 2.1% of ^{18}F-FDG PET/CT scans performed in men for an oncologic indication revealed incidental ^{18}F-FDG uptake in the prostate gland. Among those prostate incidentalomas, 7.5% were malignant. SUV_{max} alone was unable to differentiate between benign and malignant prostate lesions, however there was a statistically significant difference between the serum PSA of benign and malignant prostate lesions. These findings suggest that obtaining a serum PSA level in a patient with an ^{18}F-FDG positive prostate incidentaloma is a reasonable initial course of action. Patients with significantly elevated serum PSA levels can then be investigated further with biopsy, or followed non-invasively with serial PSAs, clinical examination or follow-up imaging.

Ethics

Ethics Committee Approval: Retrospective study. **Informed Consent:** Retrospective study.

Peer-review: Externally peer-reviewed.

Authorship Contributions

Concept: W.M., Design: W.M., A.C., Data Collection and Processing: A.C., Analysis or Interpretation: W.M., A.C., Literature Search: W.M., A.C., Writing: W.M., A.C.

Conflict of Interest: No conflict of interest was declared by the authors.

Financial Disclosure: The authors declared that this study received no financial support.

References

1. Cook GJ, Fogelman I, Maisey MN. Normal physiological and benign pathological variants of 18-fluoro-2-deoxyglucose positron emission tomography scanning: potential for error in interpretation. Semin Nucl Med 1996;26:308-314.
2. Bakheet SM, Powe J. Benign causes of 18-FDG uptake on whole body imaging. Semin Nucl Med 1998;28:352-358.
3. Kostakoglu L, Hardoff R, Mirtcheva R, Goldsmith SJ. PET-CT fusion imaging in differentiating physiologic from pathologic FDG uptake. Radiographics 2004;24:1411-1431.
4. Israel O, Yefremov N, Bar-Shalom R, Kagana O, Frenkel A, Keidar Z, Fischer D. PET/CT detection of unexpected gastrointestinal foci of 18F-FDG uptake: incidence, localization patterns, and clinical significance. J Nucl Med 2005;46:758-762.
5. Tatlidil R, Jadvar H, Bading JR, Conti PS. Incidental colonic fluorodeoxyglucose uptake: correlation with colonoscopic and histopathologic findings. Radiology 2002;224:783-787.

6. Litmanovich D, Gourevich K, Israel O, Gallimidi Z. Unexpected foci of 18F-FDG uptake in the breast detected by PET/CT: incidence and clinical significance. Eur J Nucl Med Mol Imaging 2009;36:1558-1564.
7. Choi JY, Lee KS, Kim HJ, Shim YM, Kwon OJ, Park K, Baek CH, Chung JH, Lee KH, Kim BT. Focal thyroid lesions incidentally identified by integrated 18F-FDG PET/CT: clinical significance and improved characterization. J Nucl Med 2006;47:609-615.
8. Kang BJ, Lee JH, Yoo Ler, Kim SH, Choi JJ, Jeong SH, Yim HW. Clinical significance of incidental finding of focal activity in the breast at 18F-FDG PET/CT. AJR 2011;197:341-347.
9. Metser U, Miller E, Lerman H, Lievshitz G, Avital S, Even-Sapir E. 18F-FDG PET/CT in the evaluation of adrenal masses. J Nucl Med 2006;47:32-37.
10. Basu S, Houseni M, Alavi A. Significance of incidental fluorodeoxyglucose uptake in the parotid glands and its impact on patient management. Nucl Med Commun 2008;29:367-373.
11. Han EJ, H O J, Choi WH, Yoo IR, Chung SK. Significance of incidental focal uptake in prostate on 18-fluoro-2-deoxyglucose positron emission tomography CT images. Br J Radiol 2010;83:915-920.
12. Cho SK, Choi JY, Yoo J, Cheon M, Lee JY, Hyun SH, Lee EJ, Lee KH, Kim BT. Incidental focal 18F-FDG uptake in the prostate: clinical significance and differential diagnostic criteria. Nucl Med Mol Imaging 2011;45:192-196.
13. Bhosale P, Balachandran A, Vikram R, Viswanathan C, Macapinlac H, Rohren E, Prativadi R. What is the clinical significance of FDG unexpected uptake in the prostate in patients undergoing PET/CT for other malignancies? Int J Mol Imaging 2013;2013:476786.
14. Hwang I, Chong A, Jung SI, Hwang EC, Kim SO, Kang TW, Kwon DD, Park K, Ryu SB. Is further evaluation needed for incidental focal uptake in the prostate in 18-fluoro-2-deoxyglucose positron emission tomography-computed tomography images? Ann Nucl Med 2013;27:140-145.
15. Seino H, Ono S, Miura H, Morohashi S, Wu Y, Tsushima F, Takai Y, Kijima H. Incidental prostate 18F-FDG uptake without calcification indicates the possibility of prostate cancer. Oncol Rep 2014;31:1517-1522.
16. Kang PM, Seo WI, Lee SS, Bae SK, Kwak HS, Min K, Kim W, Kang DI. Incidental abnormal FDG uptake in the prostate on 18-fluoro-2-deoxyglucose positron emission tomography-computed tomography scans. Asian Pac J Cancer Prev 2014;15:8699-8703.
17. Yang Z, Hu S, Cheng J, Xu J, Shi W, Zhu B, Zhang Y, Yao Z, Pan H, Zhang Y. Prevalence and risk of cancer of incidental uptake in prostate identified by fluorine-18 fluorodeoxyglucose positron emission tomography/computed tomography. Clin Imaging 2014;38:470-474.
18. Kao PF, Chou YH, Lai CW. Diffuse FDG uptake in acute prostatitis. Clin Nucl Med 2008;33:308-310.
19. Lawrentschuk N, Davis ID, Bolton DM, Scott AM. Positron emission tomography and molecular imaging of the prostate: an update. BJU Int 2006;97:923-931.
20. Hayasaka K, Koyama M, Fukui I. FDG-PET imaging in a patient with primary seminoma of the prostate. Clin Nucl Med 2011;36:593-594.
21. Goto T, Maeshima A, Oyamada Y, Kato R. Solitary pulmonary metastasis from prostate sarcomatoid cancer. World J Surg Oncol 2010;19:101.
22. Liu Y. FDG-PET-CT demonstration of metastatic neuroendocrine tumor of the prostate. World J Surg Oncol 2008;6:64.
23. Takahashi N, Inoue T, Lee J, Yamaguchi T, Shizukuishi K. The roles of PET and PET/CT in the diagnosis and management of prostate cancer. Oncology 2007;72:226-233.
24. Loeb S, Gashti SN, Catalona WJ. Exclusion of inflammation in the differential diagnosis of an elevated prostate-specific antigen (PSA). Urol Oncol 2009;27:64-66.
25. Serretta V, Catanese A, Daricello G, Liotta R, Allegro R, Martorana A, Aragona F, Melloni D. PSA reduction (after antibiotics) permits to avoid or postpone prostate biopsy in selected patients. Prostate Cancer Prostatic Dis 2008;11:148-152.
26. Catalona WJ, Partin AW, Slawin KM, Brawer MK, Flanigan RC, Patel A, Richie JP, deKernion JB, Walsh PC, Scardino PT, Lange PH, Subong EN, Parson RE, Gasior GH, Loveland KG, Southwick PC. Use of the percentage of free prostate-specific antigen to enhance differentiation of prostate cancer from benign prostatic disease: a prospective multicenter clinical trial. JAMA 1998;279:1542-1547.
27. Lee R, Localio AR, Armstrong K, Malkowicz SB, Schwartz JS; Free PSA Study Group. A meta-analysis of the performance characteristics of the free prostate-specific antigen test. Urology 2006;67:762-768.
28. Catalona WJ, Southwick PC, Slawin KM, Partin AW, Brawer MK, Flanigan RC, Patel A, Richie JP, Walsh PC, Scardino PT, Lange PH, Gasior GH, Loveland KG, Bray KR. Comparison of percent free PSA, PSA density, and age-specific PSA cutoffs for prostate cancer detection and staging. Urology 2000;56:255-260.
29. Aksoy Y, Oral A, Aksoy H, Demirel A, Akcay F. PSA density and PSA transition zone density in the diagnosis of prostate cancer in PSA gray zone cases. Ann Clin Lab Sci 2003;33:320-323.
30. Horninger W, Reissigl A, Klocker H, Rogatsch H, Fink K, Strasser H, Bartsch G. Improvement of specificity in PSA-based screening by using PSA-transition zone density and percent free PSA in addition to total PSA levels. Prostate 1998;37:133-137.
31. Shiiba M, Ishihara K, Kimura G, Kuwako T, Yoshihara H, Sato H, Kondo Y, Tsuchiya S, Kumita S. Evaluation of primary prostate cancer using 11C-methionine-PET/CT and 18F-FDG PET/CT. Ann Nucl Med 2012;26;138-145.
32. Richter JA, Rodriguez M, Rioja J, Penuelas I, Marti-Climent J, Garrastachu P, Quincoces G, Zudaire J, Garcia-Velloso MJ. Dual tracer 11C-choline and FDG-PET in the diagnosis of biochemical prostate cancer relapse after radical treatment. Mol Imaging Biol 2010;12:210-217.
33. Eiber M, Maurer T, Souvatzoglou M, Beer AJ, Ruffani A, Haller B, Graner FP, Kübler H, Haberhorn U, Eisenhut M, Wester HJ, Gschwend JE, Schwaiger M. Evaluation of hybrid 68Ga-PSMA ligand PET/CT in 248 patients with biochemical recurrence after radical prostatectomy. J Nucl Med 2015;56:668-674.
34. Koulikov V, Barnes S, Even-Sapir E. 68Ga-PSMA PET-CT in patients with newly diagnosed high-risk prostate cancer. J Nucl Med 2016;57(Suppl 2):1540.
35. Uprimny C, Kroiss AS, Decristoforo C, Fritz J, von Guggenberg E, Kendler D, Scarpa L, di Santo G, Roig LG, Maffey-Steffan J, Horninger W, Virgolini IJ. 68Ga-PSMA-11 PET/CT in primary staging of prostate cancer: PSA and Gleason score predict the intensity of tracer accumulation in the primary tumor. Eur J Nucl Med Mol Imaging 2017.